



# OMPS-LP aerosol extinction coefficients and their applicability in GloSSAC

Mahesh Kovilakam<sup>1,2</sup>, Larry W. Thomason<sup>2</sup>, Magali Verkerk<sup>3</sup>, Thomas Aubry<sup>3</sup>, and Travis N. Knepp<sup>2</sup>

<sup>1</sup>ADNET Systems Inc, Bethesda, MD, USA

<sup>2</sup>NASA Langley Research Center, Hampton, VA, USA

<sup>3</sup>Department of Earth and Environmental Sciences, University of Exeter, Penryn, UK

**Correspondence:** Mahesh Kovilakam (mahesh.kovilakam@nasa.gov)

Received: 30 July 2024 – Discussion started: 2 August 2024

Revised: 8 November 2024 – Accepted: 11 November 2024 – Published: 16 January 2025

**Abstract.** The Global Space-based Stratospheric Aerosol Climatology (GloSSAC) is essential for understanding and modeling the climatic impacts of stratospheric aerosols. It relies primarily on data from the Stratospheric Aerosol Gas Experiment (SAGE) satellite series, supplemented by the Optical Spectrograph and Infrared Imaging System (OSIRIS) and Cloud-Aerosol Lidar and Infrared Pathfinder Satellite Observations (CALIPSO). GloSSAC currently provides stratospheric aerosol extinction coefficients and aerosol optical depths at 525 and 1020 nm. With CALIPSO decommissioned and OSIRIS nearing the end of its operational life, SAGE III/ISS (International Space Station) will soon become the sole data source for GloSSAC, but it will only be available as long as the ISS is operational, until around 2030. Therefore, incorporating other measurements, such as those from the Ozone Mapping and Profiler Suite Limb Profiler (OMPS-LP), is critical. OMPS-LP has provided continuous aerosol extinction coefficient measurements since 2012 with a retrieval algorithm developed by NASA, i.e., OMPS(NASA). However, OMPS(NASA) has been shown to overestimate aerosol extinction coefficients, particularly after the 2022 Hunga Tonga eruption, compared to the tomographic retrieval of OMPS developed by the University of Saskatchewan (OMPS(SASK)) and SAGE III/ISS. Our analysis shows that OMPS(NASA) indeed exhibits a consistently high bias ( $> 50\%$ ) following large volcanic eruptions and pyrocumulonimbus plumes from intense wildfires, while OMPS(SASK) shows reasonable agreement with SAGE III/ISS between  $40^\circ$  S and  $40^\circ$  N. This overestimation by OMPS(NASA) leads to an overestimation of the aerosol effective radiative forcing (ERF) and the associated model-simulated global surface temperature response by a factor of about 2.

## 1 Introduction

Stratospheric aerosols play a crucial role in influencing the radiative and chemical equilibrium of Earth's atmosphere, in part due to their episodic enhancements associated with volcanic activity that can almost instantaneously enhance the total mass of aerosol in the stratosphere by several orders of magnitude (e.g., Thomason and Vernier, 2013). As a result, constraining stratospheric aerosol radiative forcing and understanding its climatic impacts is a major focus of many climate studies (e.g., Lacis et al., 1992; Myhre et al., 2013; Zanchettin et al., 2016; Timmreck et al., 2018; Krishnamohan et al., 2019). Stratospheric aerosols are key forc-

ings in the 6th phase of the Coupled Model Intercomparison Project (CMIP6) of the World Climate Research Programme (WCRP) (Eyring et al., 2016) as well as the ongoing 7th phase (CMIP7). Most global climate models (GCMs) participating in CMIP do not simulate the stratospheric aerosol life cycle interactively from emissions; instead, they rely on prescribed aerosol optical properties based on global measurements (Stenchikov et al., 2006; Berdahl and Robock, 2013; Fyfe et al., 2013). GCMs with interactive stratospheric aerosols also often employ measurements to help evaluate their simulations (Aquila et al., 2013; Mills et al., 2016; Timmreck et al., 2018). To serve these needs, the Global Space-based Stratospheric Aerosol Climatology (GloSSAC)

was first released in 2018 (Thomason et al., 2018). It is an outgrowth of the SPARC Assessment of Stratospheric Properties (ASAP) and is an extensive multi-sensor climatology of stratospheric aerosol optical properties since 1979 that has been widely used by atmospheric modeling groups. It has played a crucial role in validating interactive aerosol schemes (e.g., Timmreck et al., 2018; Quaglia et al., 2023) and developing simple aerosol models that can be applied to provide aerosol optical properties to GCMs without interactive schemes (Aubry et al., 2020). GloSSAC consists primarily of visible and near-infrared aerosol extinction coefficient values in a monthly 5° latitude and 0.5 km altitude grid that currently extends, as of version 2.22, from 1979 through 2023 (NASA/LARC/SD/ASDC, 2024).

Stratospheric Aerosol and Gas Experiment (SAGE) measurements provide the backbone of GloSSAC and are available from 1979 to 1981 (SAGE), 1984 to 2005 (SAGE II), and 2017 to the present (SAGE III/ISS – International Space Station). Breaks in these time periods are filled with a combination of other space-based data, point-based data sets including lidar and balloon-borne instruments, and aircraft data (Thomason et al., 2018; Kovilakam et al., 2020). The “filling” of missing data also includes the aftermath of the Mt. Pinatubo eruption, where SAGE II observations were not possible in the lower stratosphere for several years. Improving this filling process remains the focus of ongoing research efforts. In the 2005–2017 gap, single-wavelength measurements by the Optical Spectrograph and Infrared Imaging System (OSIRIS) and Cloud-Aerosol Lidar with Orthogonal Polarization (CALIOP) were employed to fill the void (Thomason et al., 2018; Kovilakam et al., 2020). One disadvantage is that measurements of the aerosol extinction coefficients at multiple wavelengths are crucial for inferring aerosol properties, which is a primary application of GloSSAC data. Another issue is that the quality of even the single-channel data degrades during a number of small to moderate volcanic eruptions and intrusions of smoke during this period. While GloSSAC incorporates data from multiple sensors, its limitations must also be acknowledged. Solar occultation measurements, such as SAGE, are relatively straightforward measurements that are robust over a large range of stratospheric aerosol levels and provide near-global coverage. However, the measurement rate is slow and full zonal coverage requires about a month. In contrast, OSIRIS and CALIPSO offer daily near-global aerosol measurements, opening up a broad range of potential research opportunities not provided by solar occultation. They are, however, limited in data quality by a retrieval process that relies on assumptions about aerosol microphysical properties, particularly size distribution and composition (e.g., Bourassa et al., 2012; Rieger et al., 2015, 2019; Kar et al., 2019). For the 2005–2017 gap in SAGE coverage and as a supplement in other periods, a conformance process has been implemented in GloSSAC (Kovilakam et al., 2020), serving as a mechanism to remove instrument-to-instrument bias. During pe-

riods when the OSIRIS and CALIOP instruments had temporal overlap with a SAGE instrument, this conformance process revealed that both data sets varied in their consistency when converting to the standard GloSSAC measurement wavelengths. This variation could be substantial and extends beyond variations associated with aerosol properties alone, particularly following volcanic and smoke events (Kovilakam et al., 2020).

With the end of the CALIPSO mission in 2023 and the impending end of OSIRIS’s operational lifespan, only SAGE III/ISS will remain among the current ensemble of instruments used to create GloSSAC in the future. Realistically, even this instrument cannot be expected to survive much beyond 2030 or whenever the ISS is de-orbited ( $\approx 2030$ ). It is worth noting that there are currently no plans among the various space agencies to fly a solar occultation instrument in the future. As a result, our ability to extend GloSSAC into the future hinges on identifying a set of measurements that will be available and have sufficient data quality and comparable spatial and temporal coverage. One obvious possibility is the Ozone Mapping and Profiler Suite (OMPS), which has been operational since 2012 with additional flights sufficient to extend its observations into the foreseeable future. This data set is available from two different groups using different retrieval approaches. OMPS(NASA) provides aerosol extinction coefficient retrievals at six wavelengths (510, 600, 675, 745, 869, and 997 nm) in version 2.1 (Taha et al., 2021). The University of Saskatchewan offers a tomographic version of the OMPS retrieval, OMPS(SASK), which produces the aerosol extinction coefficient data at only 745 nm. These data sets are generally in good agreement in background periods; however, large differences between the OMPS(NASA) and OMPS(SASK) products occur following events like the Hunga Tonga eruption in January 2022 (Bourassa et al., 2023). Similar differences have been observed following other perturbations to stratospheric aerosol levels, including the 2019/2020 Australian bush fires. The Hunga Tonga event is of particular interest because it is one of the largest stratospheric events since that of Mt. Pinatubo in 1991 and because it is an event during which the aerosol extinction coefficient measurements by OMPS, SAGE II-I/ISS, and OSIRIS exhibit differences.

Our goal in this paper is to examine and evaluate the two different products of OMPS data, OSIRIS and SAGE III/ISS, following the Hunga Tonga eruption and other stratospheric aerosol events since 2017. Ultimately, we aim to assess the best retrieval approach for integrating OMPS data into GloSSAC in the future without relying on constraining solar occultation observations. We will also assess the potential limitations of using these data sets to depict future volcanic and smoke events in order to understand the degree to which the GloSSAC data quality will be affected by this change.

## 2 Data and methods

### 2.1 OMPS

The OMPS Limb Profiler (OMPS-LP) is a component of the Suomi National Polar-orbiting Partnership (Suomi NPP) satellite and the Joint Polar Satellite System (JPSS) satellites launched in October 2011 (Flynn et al., 2006). While its primary focus is on monitoring the vertical structure of the ozone layer, OMPS-LP utilizes the limb-scatter technique to retrieve information about aerosols and related gases. Operating in a midday Sun-synchronous orbit, OMPS provides near-global coverage on a daily basis.

The retrieval methodology employed in OMPS-LP version 2.0, referred to as OMPS(NASA), involves establishing a one-to-one correspondence between a single limb radiance image and the retrieval of a singular aerosol extinction coefficient profile. This approach assumes horizontal homogeneity of the atmosphere along the line of sight. The retrieval is carried out across six spectral bands at 510, 600, 675, 745, 869, and 997 nm (Taha et al., 2021). In the latest iteration (version 2.1), the incorporation of more comprehensive convergence checks has improved the retrieval process, especially in the presence of volcanic plumes (Taha et al., 2022). Similar to other limb-scatter measurements, the OMPS(NASA) procedure requires an assumption regarding the particle size distribution for deriving the scattering phase function. In the case of OMPS(NASA), a constant gamma function size distribution derived from the Community Aerosol and Radiation Model for Atmospheres (CARMA) is utilized with  $\alpha = 1.8$  and  $\beta = 20.5$ , where  $\alpha$  and  $\beta$  are the shape parameter and rate parameter, respectively (Chen et al., 2018). We utilize version 2.1 of the OMPS(NASA) product for the analyses.

OMPS-LP's imaging and rapid sampling capabilities facilitate the merging of consecutive limb images to create a two-dimensional retrieval of the aerosol extinction coefficient. This method captures the aerosol extinction coefficient simultaneously in altitude and along the orbit track. The University of Saskatchewan utilizes this ability to produce an alternative version of the OMPS data products – in the following referred to as OMPS(SASK) – in a tomographic retrieval approach. The limb-scatter tomographic retrieval using OMPS-LP measurements was initially developed by Zawada et al. (2018). While this algorithm initially focused on ozone, it also incorporated the preliminary retrieval of the aerosol extinction coefficient. The aerosol extinction coefficient is reported at 745 nm, featuring a vertical resolution of 1 km and a horizontal span of 125 km. Similar to other limb-scatter retrievals, this algorithm operates based on assuming a particle size distribution, in this instance employing a single-mode lognormal size distribution with  $r_i = 0.08$  and  $\sigma = 1.6$ , where  $r_i$  is the median radius and  $\sigma$  is the distribution width. For our study, we will utilize version 1.3 of OMPS(SASK). Another alternative version of OMPS data has been developed by the IUP, University of

Bremen (Rozanov et al., 2024), and may be considered for use in GloSSAC in the future.

### 2.2 OSIRIS

OSIRIS, a limb-scatter instrument launched aboard the Odin satellite in 2001, retrieves O<sub>3</sub>, NO<sub>2</sub>, and aerosol extinction coefficient data (McLinden et al., 2012). Odin is positioned in a Sun-synchronous orbit providing coverage from 82° S to 82° N, excluding polar winter due to insufficient sunlight for measurements. The Optical Spectrograph instrument operates within the wavelength range of 284 to 810 nm with an approximate 1 nm resolution. A typical scan takes about 90 s, offering a vertical resolution of about 1 km and resulting in 100 to 400 profiles a day. The aerosol extinction coefficient retrieval is performed at 750 nm following a multiplicative relaxation technique, as detailed in Bourassa et al. (2012).

For GloSSAC, OSIRIS version 7.2 is currently used and plays a vital role in bridging the gap between the SAGE II period (1984–2005) and the SAGE III/ISS mission (June 2017–present). Significant improvements have been made to the version 7.2 data (Rieger et al., 2019) compared to the version 5.07 data (Bourassa et al., 2012). The retrieval in version 7.2 enhances the accuracy of the aerosol extinction coefficient product by minimizing the sensitivity to the unknown particle size distribution during inversion. This version aligns more closely with SAGE II and SAGE III/ISS compared to the previous version (v5.07) in GloSSAC version 1.0. While the mission is ongoing, limitations in instrument operations have reduced the overall number of measurements made per orbit and concomitantly affect the latitudinal coverage. Additionally, following the Hunga Tonga eruption, the OSIRIS aerosol extinction coefficient is about 50 % lower than that measured by SAGE III/ISS during this period. This discrepancy remains under study by the OSIRIS team<sup>1</sup>.

### 2.3 SAGE III/ISS

SAGE III/ISS utilizes the solar occultation technique (McCormick et al., 1979), which measures the attenuation of solar radiation caused by the scattering and absorption of atmospheric constituents during sunrise and sunset events. SAGE III/ISS commenced data collection in June 2017 and represents an upgraded version of SAGE III on the Meteor (SAGE III/M3M) instrument. Operating in a manner akin to its predecessors (e.g., Mauldin et al., 1985; Thomason et al., 2010), SAGE III/ISS retrieves vertical profiles of multiwavelength aerosol extinction coefficients (384, 449, 521, 602, 676, 756, 864, 1022, and 1544 nm), along with gas-phase species. The SAGE instrument family, renowned for its high precision (< 5 %), has a legacy of providing vertical profiles of global

<sup>1</sup>The OSIRIS team is actively investigating potential causes of underestimation, examining assumptions regarding size distribution in the retrieval algorithm and the impact of plume altitude on stray light (Adam Bourassa, personal communication).

stratospheric aerosols. These profiles serve as a benchmark for various correlative measurements, facilitating comparisons and validation (e.g., Hervig and Deshler, 2002; Deshler et al., 2003, 2019; Rieger et al., 2019; Bourassa et al., 2019). Due in part to a relatively straightforward process for inferring mid-visible to near-infrared measurements especially of the aerosol extinction coefficients, we consider observations by this instrument to be the standard against which other approaches are evaluated. Furthermore, the SAGE series of measurements play a crucial role in creating GloSSAC, in conjunction with other space-based observations (Thomason et al., 2018; Kovilakam et al., 2020).

We have utilized version 5.3 of the SAGE III/ISS data for all the analyses detailed in this paper. The modifications introduced in version 5.3 are outlined in the release notes available at [https://asdc.larc.nasa.gov/documents/sageiii-iss/guide/ReleaseNotes\\_G3B\\_v05.30.pdf](https://asdc.larc.nasa.gov/documents/sageiii-iss/guide/ReleaseNotes_G3B_v05.30.pdf) (last access: 2 January 2025). Notable changes in the solar product in version 5.3 encompass Disturbance Monitoring Package (DMP) corrections specifically applied to solar products and a shift to using Modern-Era Retrospective analysis for Research and Applications Version 2 (MERRA-2) 72-layer data for meteorological input. While SAGE III/ISS aerosol extinction coefficient measurements have been extensively employed for validation, comparison, and long-term climatology purposes (e.g., Bourassa et al., 2019; Rieger et al., 2019; Kar et al., 2019; Kovilakam et al., 2020), a negative bias has been observed in the aerosol channels (521, 602, and 676 nm) close to the Chappuis ozone absorption band in the version 5.2 aerosol data (Wang et al., 2020). Caution is advised when using these aerosol extinction coefficient measurements at the above wavelengths due to the reported bias, and ongoing investigations are being conducted to address this issue.

## 2.4 Modeling of effective radiative forcing and the associated surface temperature response

To assess the importance of differences between the aerosol optical property data sets considered in this study, we estimate the global mean effective radiative forcing (ERF) and the associated temperature response for each data set. To estimate the global mean ERF, we use the relationship from Marshall et al. (2020):

$$\text{ERF} = -20.7 \times (1 - e^{-\Delta\text{SAOD}}), \quad (1)$$

where  $\Delta\text{SAOD}$  is the global mean 550 nm stratospheric aerosol optical depth (SAOD) anomaly. We calculate this anomaly as the deviation of SAOD from its minimum over 2017–2023. Due to spatial coverage limitations, and to preserve the temporal resolution of the SAOD time series, we apply this relationship to the monthly 60°S–60°N mean  $\Delta\text{SAOD}$  instead of the annual global mean used by Marshall et al. (2020) for the calibration of Eq. (1). We assume that this approximation still provides a reasonable estimate of the global mean ERF. Previous studies have typically assumed

a linear relationship between ERF and SAOD, with Forster et al. (2021) estimating a best value of  $-20 \pm 5 \text{ W m}^{-2}$  per unit SAOD for the proportionality factor. Using a nonlinear relationship better reflects the expected physical relationship between radiative forcing and SAOD and accurately captures the ERF–SAOD relationship in an extensive set of stratospheric aerosol injection simulations with the UM-UKCA interactive stratospheric aerosol model (Marshall et al., 2020).

To calculate the global mean surface temperature response associated with each stratospheric aerosol data set, we use the Finite-amplitude Impulse Response (FaIR) model, a three-box impulse response model designed to mimic the behavior of complex Earth system models (ESMs) (Millar et al., 2017; Smith et al., 2018; Leach et al., 2021). This model transforms emissions of greenhouse gases and short-lived climate forcers into a concentration and radiative forcing time series, which is then used to estimate global temperature anomalies. We performed six 1000-member ensembles corresponding to the five aerosol optical property data sets used in our study, i.e., OMPS(NASA), OMPS(SASK), OSIRIS, SAGE III/ISS, and GloSSAC, plus an ensemble with no stratospheric-aerosol-induced ERF. Each member is run with FaIR at a monthly resolution with a different set of parameters (heat capacity, heat exchange coefficient for each box, climate feedback parameter, and forcing efficacy), effectively quantifying the climate modeling uncertainty. We run each ensemble with climate forcings from the Reduced Complexity Model Intercomparison Project (Nicholls et al., 2021), replacing the volcanic forcing time series with the ERF time series calculated from Eq. (1) using the SAOD time series corresponding to each aerosol optical property data set tested. We do not propagate uncertainty related to climate variability, SAOD uncertainty, or SAOD-to-ERF conversion to keep the focus on differences between the stratospheric aerosol data sets and the expected mean temperature response.

## 3 Results

For consideration in GloSSAC, all data sets are required to be publicly available at a recognized data center and to have undergone peer-reviewed validation for their stratospheric aerosol products, among other requirements (Thomason et al., 2018). Both the OMPS(NASA) (Taha et al., 2021, 2022) and OMPS(SASK) (Bourassa et al., 2023) products satisfy these criteria, and both are valid, albeit competing, candidates for integration into the GloSSAC framework.

### 3.1 Evaluation of the OMPS aerosol extinction coefficient at 745 nm within the GloSSAC framework

Given the variations in measurement frequency and coverage across the instruments, we utilize zonally averaged daily measurements to facilitate meaningful comparisons. Our analysis focuses on the aerosol extinction coefficient data at 745 nm from OMPS(NASA) and OMPS(SASK) and

at 750 nm from OSIRIS, starting from January 2012 when OMPS data became available and extending to SAGE II-ISS measurements from June 2017 to the present. We opt to compare daily zonally averaged profiles from each instrument within a  $4^\circ$  latitude band, ensuring ample data for statistical analysis. Figure 1a illustrates daily zonally averaged aerosol extinction coefficient profiles for OMPS(NASA), OMPS(SASK), and OSIRIS, representing a relatively unperturbed period (28 March 2013). The horizontal bars in the aerosol extinction coefficient profiles depict a  $\pm 1$  standard deviation of the averaged profiles. The averaged aerosol extinction coefficient profiles for 28 March 2013 in the latitude band  $30\text{--}34^\circ$  N from each instrument exhibit good agreement above the tropopause, as shown in the percent difference plot in Fig. 1a. Percent differences remain mostly within  $\pm 20\%$  between the tropopause and 25 km, suggesting reasonable agreement between OMPS(NASA), OMPS(SASK), and OSIRIS for a period with relatively low aerosol levels. Notably, differences in the scale of 20% are relevant to GloSSAC (Thomason et al., 2018; Kovilakam et al., 2020), provided the behavior of each instrument remains consistent and that they vary systematically. Therefore, aerosol profiles during periods of low aerosol loading appear to be satisfactory in the context of GloSSAC. However, during perturbed periods, such as those caused by recent volcanic or smoke events, results may differ significantly, as observed following the Kelud volcanic eruption on 13 February 2014 at  $8^\circ$  S and the Calbuco volcanic eruption on 28 April 2015 at  $41^\circ$  S.

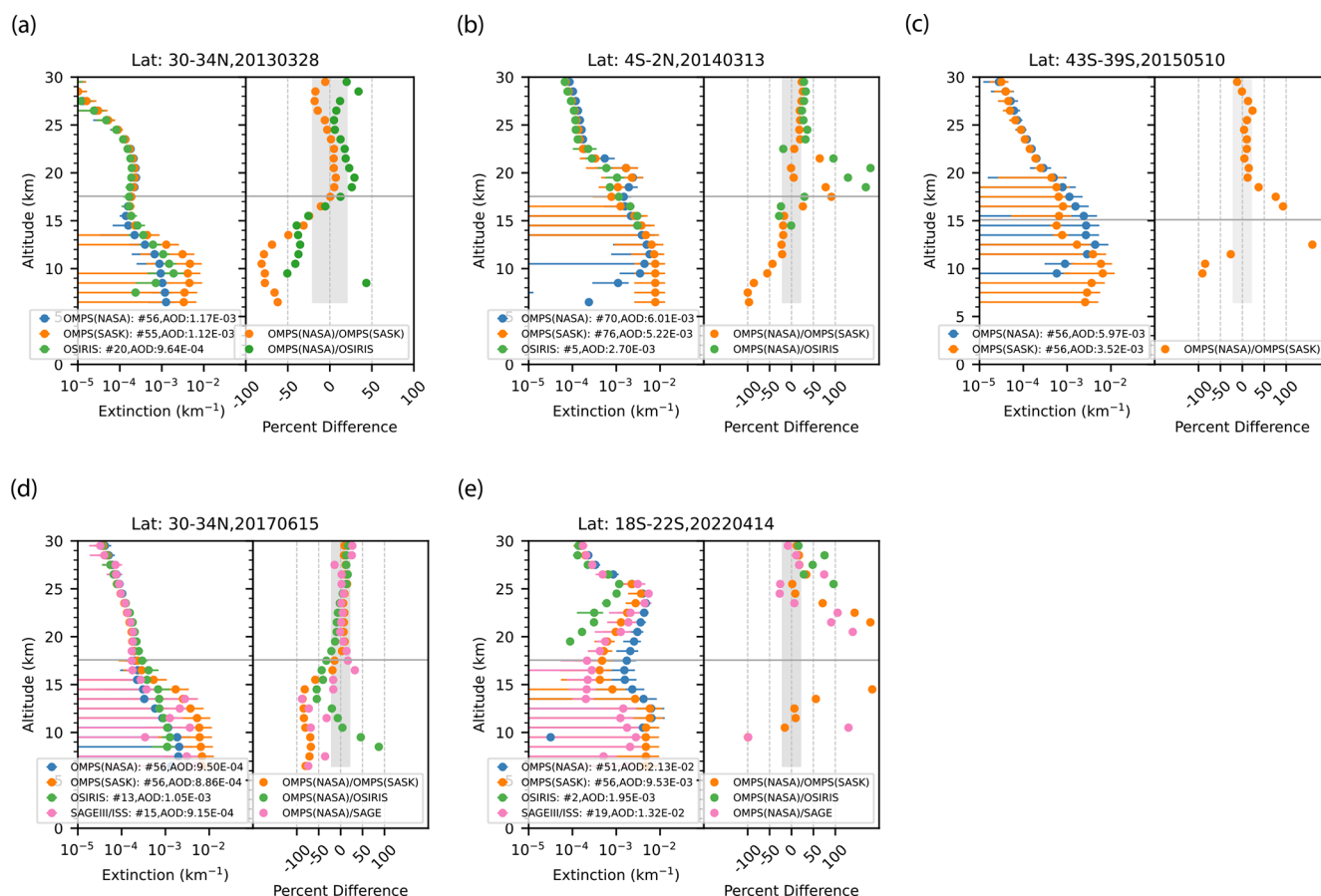
Figure 1b presents daily zonally averaged aerosol extinction coefficient profiles for OMPS(NASA), OMPS(SASK), and OSIRIS following the Kelud eruption. The averaged aerosol extinction coefficient profiles for 13 March 2014 in the latitude band  $4^\circ$  S– $2^\circ$  N from each instrument reveal differences between the tropopause and approximately 23 km, where volcanic aerosol loading is evident. In this case, the difference not only exceeds the permissible difference criterion of  $\pm 20\%$  used for GloSSAC but also frequently exceeds 50% and occasionally even more, far surpassing the acceptable bounds. While the SAODs from OMPS(NASA) and OMPS(SASK) do not exhibit significant differences, the SAOD difference between OMPS(NASA) and OSIRIS is notably distinct by more than 70%.

Figure 1c illustrates daily zonally averaged aerosol extinction coefficient profiles following the Calbuco eruption for OMPS(NASA) and OMPS(SASK). The averaged aerosol extinction coefficient profiles for 10 April 2015 in the latitude band  $43\text{--}39^\circ$  S from each instrument show differences between the tropopause and 18 km, where volcanic aerosol loading is evident. This contrast is highlighted in Fig. 1c, illustrating percent differences between OMPS(NASA) and OMPS(SASK) exceeding 70%. Furthermore, the SAOD from OMPS(NASA) significantly exceeds that of OMPS(SASK) by more than 50% as data between the tropopause and 18 km contribute more towards this difference, as is evident from the percent difference plots. No

measurements are available from OSIRIS for this comparison.

We also conducted an analysis of the aerosol extinction coefficient data from OMPS(NASA) and OMPS(SASK) at 745 nm, starting from June 2017, when the corresponding measurements were available from SAGE III/ISS. While reasonable agreement between OMPS(NASA), OMPS(SASK), and SAGE III/ISS (within  $\pm 20\%$ ) is seen during relatively unperturbed periods in the stratosphere such as June 2017 (Fig. 1d), the scenario is completely different following the volcanic eruption of Hunga Tonga on 15 January 2022 at  $21^\circ$  S, and the level of agreement between the instruments degrades dramatically. Figure 1e displays the zonally averaged aerosol extinction coefficient profiles for the latitude band  $18\text{--}22^\circ$  S on 14 April 2022, revealing that OMPS(NASA) significantly overestimates the aerosol extinction coefficient by approximately 80% or more relative to OMPS(SASK) and SAGE III/ISS. This finding corroborates the results of Bourassa et al. (2023). Notably, the percent difference between the OMPS(NASA) and OMPS(SASK) versions also exhibits significant differences, although these are not as significant as those between OMPS(NASA) and SAGE II-ISS. While overestimation in the lower stratosphere (approximately between the tropopause and about 20 km for the tropics) is a known issue for limb-scatter measurements that is mainly attributable to cloud contamination at these altitudes (Rieger et al., 2015; Kovilakam et al., 2020), the percent difference between OMPS(NASA)/OMPS(SASK) and OMPS(NASA)/SAGE III/ISS at altitudes between 25 and 20 km shows a clear overestimation within the OMPS(NASA) data set, exceeding 80% or more. Additionally, the computed SAOD between the tropopause and 25 km for the averaged aerosol extinction coefficient profile (Fig. 1e) shows that the OMPS(NASA) product (SAOD:  $2.13 \times 10^{-2}$ ) overestimated the SAOD by approximately 60% compared to both OMPS(SASK) (SAOD:  $9.53 \times 10^{-3}$ ) and SAGE III/ISS (SAOD:  $1.32 \times 10^{-2}$ ), reinforcing the fact that OMPS(NASA) overestimates the aerosol extinction coefficient below the peak, in accordance with the findings of Bourassa et al. (2023). Although we present the result from OSIRIS here for comparison purposes, due to declining coverage and low-frequency measurements in the Southern Hemisphere, OSIRIS only provides two profiles for this comparison and may not properly represent aerosol profiles in the stratosphere following the eruption. Additionally, caution must be exercised when using OSIRIS data after 2021 (Rozanov et al., 2024) due to underestimation of the aerosol extinction coefficient.

In addition to the daily zonal averages, we analyzed the zonally averaged aerosol extinction coefficient profiles from various instruments and gridded them to match GloSSAC's spatial resolution of  $5^\circ$  latitude. While other eruptions such as Kelud and Calbuco show similar significant differences between OMPS(NASA) and other measurements, here we only show an instance following the Hunga



**Figure 1.** Daily zonally averaged profiles of the aerosol extinction coefficient. OMPS(NASA) at 745 nm, OMPS(SASK) at 745 nm, OSIRIS at 750 nm, and SAGE III/ISS at 756 nm are used for comparison. The zonally averaged aerosol extinction coefficient is depicted for (a) the latitude band 30–34° N for 28 March 2013 (relatively background stratosphere), (b) the latitude band 4° S–2° N for 13 March 2014 following the Kelud volcanic eruption on 13 February 2014, (c) the latitude band 43° S–39° S for 10 May 2015 following the Calbuco volcanic eruption on 28 April 2015, (d) the latitude band 30–34° N for 15 June 2017 (relatively background stratosphere), and (e) the latitude band 18–22° S for 14 April 2022 following the Hunga Tonga eruption on 15 January 2022. The percent differences between OMPS(NASA) and other measurements for these events are shown in the adjacent plots as  $((\text{OMPS(NASA)} - \text{other}) / \text{other}) \times 100$ . The gray-shaded region in the percent difference plot indicates the permissible discrepancies between the instruments ( $\pm 20\%$ ) within the framework of GloSSAC. The error bars in the aerosol extinction coefficient profiles represent the aerosol extinction coefficient  $\pm 1$  standard deviation. The number of profiles used to average the aerosol extinction coefficient profiles is also shown as “#”. The horizontal line represents the tropopause height. SAOD is computed by vertically integrating the aerosol extinction coefficient between the tropopause and 25 km.

Tonga eruption on 15 January 2022 for which all measurements were available. Figure 2a–d illustrate the zonally averaged aerosol extinction coefficient from OMPS(NASA), OMPS(SASK), OSIRIS, and SAGE III/ISS for April 2022 following the Hunga Tonga eruption. Figure 2e distinctly shows a significant difference for OMPS(NASA) that exceeds the aerosol extinction coefficient by 50 % or more between OMPS(NASA) and OMPS(SASK) in the latitude band 30° S–30° N and for altitudes between the tropopause and about 24 km. Similar differences are observed in Fig. 2f between OMPS(NASA) and OSIRIS. Figure 2g also reveals a significant difference between OMPS(NASA) and SAGE III/ISS. However, in addition to the overestimation of the OMPS(NASA) aerosol extinction coefficient below

the peak of the aerosol layer at about 25 km, OMPS(NASA) underestimates the aerosol extinction coefficient by about 50 % at the peak of the aerosol layer, around 25 km, within the latitude band 30° S–30° N. Similar underestimation by OMPS(SASK) is observed when comparing OMPS(SASK) to SAGE III/ISS (not shown), suggesting that underestimation at the peak of the aerosol layer by OMPS retrieval, regardless of whether this is by OMPS(NASA) or OMPS(SASK), is common for both OMPS products. This suggests that the underestimation could be attributable to the retrieval of OMPS aerosol extinction coefficients, where a fixed background size distribution assumption is used to derive the phase function (Taha et al., 2021; Bourassa et al., 2023).

The current analysis reveals a significant disparity between OMPS(NASA) and other data sets during essentially all perturbed events (e.g., Kelud, Calbuco, and Hunga Tonga). Given the permissible difference of  $\pm 20\%$  between instruments in the context of the GloSSAC framework (Thomason et al., 2018; Kovilakam et al., 2020), OMPS(NASA) significantly exceeds the bounds that are relevant to GloSSAC.

In addition to the aerosol extinction coefficient comparison, SAODs at 745 nm are computed for the entire period from 2012 to 2022. The SAOD was computed by integrating the aerosol extinction coefficient between the tropopause and 30 km using zonally averaged gridded data. Figure 3a–d present time series plots of SAODs for OMPS(NASA) at 745 nm, OMPS(SASK) at 745 nm, OSIRIS at 750 nm, and SAGE III/ISS at 756 nm. All the SAOD time series plots show an increase in SAOD following major volcanic or fire events. However, when examining the percent differences between SAOD values from different products, notable distinctions emerge. Figure 3e illustrates the percent difference between OMPS(NASA) and OMPS(SASK), revealing significant overestimation of the OMPS(NASA) aerosol optical depth following the Calbuco volcanic eruption in April 2015, the Australian wildfire in January 2020, and the Hunga Tonga volcanic eruption in January 2022. These differences exceed 50% or more, persisting even 10 months after the Hunga Tonga eruption. While OMPS(SASK) demonstrates improved consistency following perturbed events, our analysis underscores the need for further evaluation, especially in instances of aerosol overestimation poleward of 40° S and 40° N in the OMPS(SASK) product. This discrepancy is likely due to cloud contamination in the data, as evidenced by the overestimation of the aerosol extinction coefficient in the lower stratosphere in the monthly zonally averaged gridded product (not shown). We anticipate that a more robust cloud filter will enhance accuracy in such cases. Additionally, a seasonal cycle is observed in the percent difference plot, particularly poleward of 40° S and 40° N, which could be attributed to changes in the scattering angle of OMPS. We also note significant overestimation of OMPS(SASK) between 20° S and 20° N in the first couple of years of OMPS operations (Fig. 3e), which could be attributed to changes in the Level-1 OMPS product. The OMPS(SASK) team is currently investigating this issue, including the potential to move the retrieval wavelength to 869 nm, which does not appear to have these issues (Adam Bourassa, personal communication).

A notable overestimation of OMPS(NASA) SAOD is also evident when computing percent differences in SAOD between OMPS(NASA) and OSIRIS. Figure 3f displays the time series of percent differences in SAOD between OMPS(NASA) and OSIRIS. The plot clearly depicts an overestimation of the OMPS(NASA) aerosol extinction coefficient following the Kelud eruption, the Australian wildfire, and the Hunga Tonga eruption. OMPS(NASA) overestimates SAOD by approximately 50% or more following these

events. The OSIRIS aerosol extinction coefficient measurements during the Hunga Tonga time period exhibit a substantial low bias and deviate from patterns observed in previous events. The potential causes of this bias, including particle size assumptions, instrumental stray light, and sampling geometry, are currently under investigation (Adam Bourassa, personal communication). Therefore, while the overestimation of the OMPS(NASA) aerosol extinction coefficient or SAOD following major events aligns with other products, the low bias from OSIRIS may have amplified the discrepancy between OMPS(NASA) and OSIRIS.

The SAOD from OMPS(NASA) at 745 nm tends to overestimate relative to SAGE III/ISS (Fig. 3g), particularly poleward of 30° S, regardless of any volcanic event. Figure 3g also depicts a significant positive bias ( $> 50\%$ ) in the southern tropics following the Hunga Tonga eruption in January 2022. This discrepancy between OMPS(NASA) and SAGE III/ISS is in agreement with previous studies (Bourassa et al., 2023). The results so far show a clear discrepancy between OMPS(NASA) and other space-based measurements, reinforcing the fact that the OMPS(NASA) aerosol extinction at 745 nm is beyond the permissible discrepancy limit ( $\pm 20\%$ ) between the instruments in the context of GloSSAC.

### 3.2 Multiwavelength aerosol extinction coefficients from OMPS(NASA) and SAGE III/ISS

Despite its lower-frequency measurements compared to limb-scatter instruments, SAGE III/ISS remains valuable with its direct multiwavelength aerosol extinction coefficient measurements, which provide important information about particle sizes, particularly when the stratosphere is perturbed (Thomason et al., 2021). The OMPS(NASA) product also provides multiwavelength aerosol measurements, offering an opportunity to evaluate OMPS(NASA).

Figure 4 illustrates the time series of percent differences in SAOD between OMPS(NASA) and SAGE III/ISS at four wavelengths. While the 510 nm channel appears to be biased high throughout the time period (Fig. 4a), regardless of any perturbed event, 745 nm shows better agreement (Fig. 4b) relative to 510 nm. However, we note a consistent overestimation ( $> 50\%$ ) of OMPS(NASA) at 745 nm poleward of 30° S. At 869 nm (Fig. 4c), the differences are similar to 745 nm, except that the overestimation of OMPS(NASA) poleward of 30° S is improved relative to 745 nm. For 997 nm, Fig. 4d depicts a different pattern compared to Fig. 4a–c, showing that the overestimation only occurs following the Canadian wildfire and the Hunga Tonga eruption. Notably, the 510, 745, 864, and 997 nm channels from OMPS(NASA) exhibit inconsistent behavior across the spectrum, behaving differently in each channel relative to the 521, 756, 864, and 1022 nm channels in SAGE III/ISS.

In the context of GloSSAC, 510 and 997 nm from OMPS(NASA) and 521 and 1022 nm from SAGE III/ISS

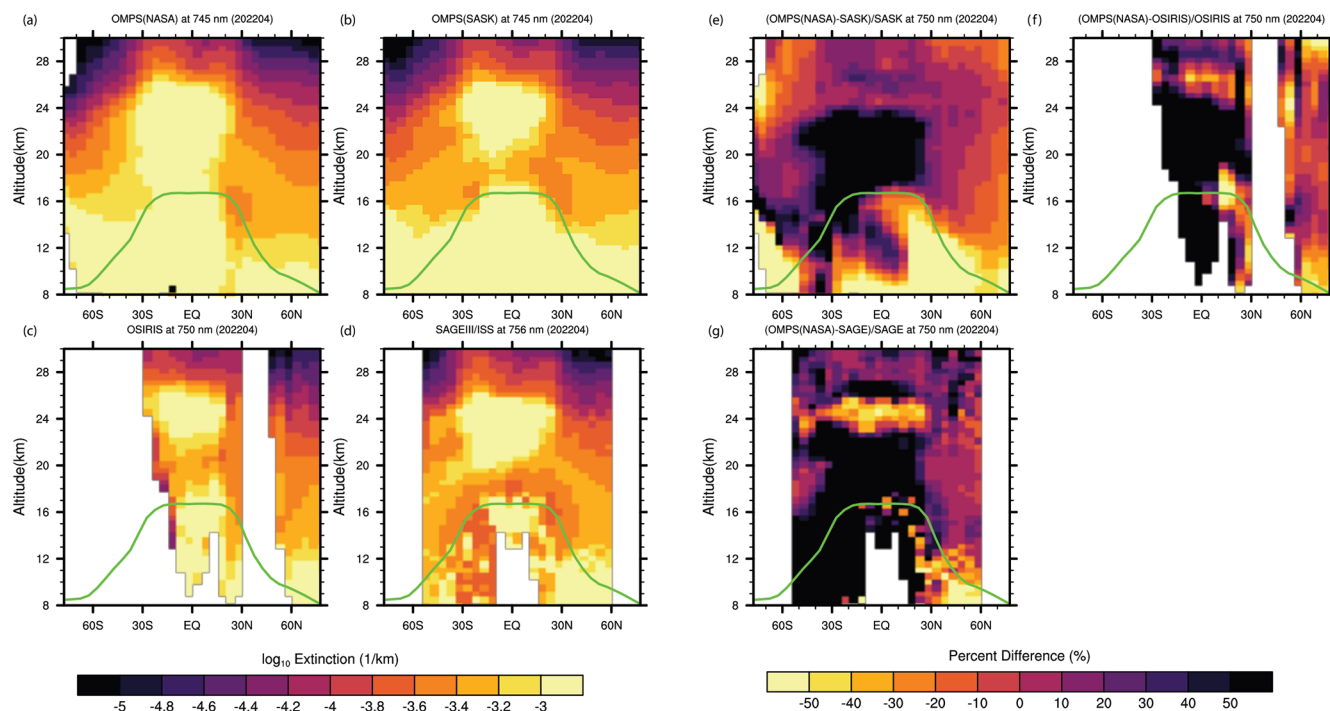


**Figure 2.** The zonally averaged gridded monthly aerosol extinction coefficient and percent difference for April 2022 following the Hunga Tonga eruption on 15 April 2022 at 21° S. **(a)** The zonally averaged aerosol extinction coefficient from OMPS(NASA) at 745 nm. **(b)** Same as panel **(a)** but for OMPS(SASK). **(c)** Same as panel **(a)** but for OSIRIS at 750 nm. **(d)** Same as panel **(a)** but for SAGE III/ISS at 756 nm. Panel **(d)** shows the percent difference of the zonally averaged aerosol extinction coefficient between OMPS(NASA) **(a)** and OMPS(SASK) **(b)**, panel **(e)** illustrates the percent difference of the zonally averaged aerosol extinction coefficient between OMPS(NASA) **(a)** and OSIRIS **(c)**, and panel **(f)** shows the percent difference between OMPS(NASA) and SAGE III/ISS. The green solid line shows the monthly averaged tropopause from OMPS(SASK).

are particularly relevant. The OMPS(NASA) product below 675 nm is not robust due to the low sensitivity of shorter wavelengths to aerosols (Taha et al., 2021). However, we use 510 nm for comparison purposes with SAGE III/ISS as GloSSAC provides an extinction coefficient at 525 nm, which is a channel close to OMPS(NASA)'s 510 nm and therefore relevant to evaluate OMPS(NASA) at 510 nm. For the analysis here, instead of examining the extinction coefficient or SAOD, we examine SAOD ratios between the channels from both OMPS(NASA) and SAGE III/ISS as extinction/SAOD ratios provide valuable information about the sizes of aerosol particles (Thomason et al., 2021; Knepp et al., 2024; Kovilakam et al., 2023). For SAGE series of measurements, 525 and 1020 nm extinction coefficient measurements are generally used to infer particle size information (Thomason et al., 2021; Knepp et al., 2024), and therefore we evaluate OMPS(NASA) 510/997 nm SAOD ratios against SAGE III/ISS 525/1020 nm SAOD ratios. Figure 5 depicts SAOD ratios computed from SAGE III/ISS (Fig. 5a) and OMPS(NASA) (Fig. 5b). An important difference between these two plots is the difference in the SAOD ratios. While following each perturbed event, the SAOD ratio from SAGE (Fig. 5a) clearly shows changes in the SAOD ratios,

particularly following the Canadian wildfire, the Raikoke eruption and the Hunga Tonga eruption, for which decreases in the SAOD ratios are observed, suggesting larger particles (Thomason et al., 2021; Knepp et al., 2024), whereas other moderate eruptions like Ambae and Ulawun show an increase in the SAOD ratios, suggesting an increased amount of smaller particles. In contrast, the OMPS(NASA) SAOD ratios (Fig. 5b) are completely inconsistent with the SAGE III/ISS values and thus unlikely to be useful for inferring any correct information regarding aerosol size. The percent difference plot between SAGE and OMPS (Fig. 5c) clearly suggests that the OMPS(NASA) SAOD ratios have a significant bias (> 50%), mostly due to the bias in the 510 nm channel as mentioned earlier, and therefore they are not suitable for GloSSAC purposes.

From the aforementioned comparisons, it is evident that OMPS(NASA) tends to overestimate the aerosol extinction coefficient and SAOD following major events in comparison to SAGE III/ISS and other space-based aerosol measurements. Moreover, the multiwavelength measurements from OMPS at 510, 745, 869, and 997 nm are inconsistent across the channels, suggesting that OMPS(NASA) multi-

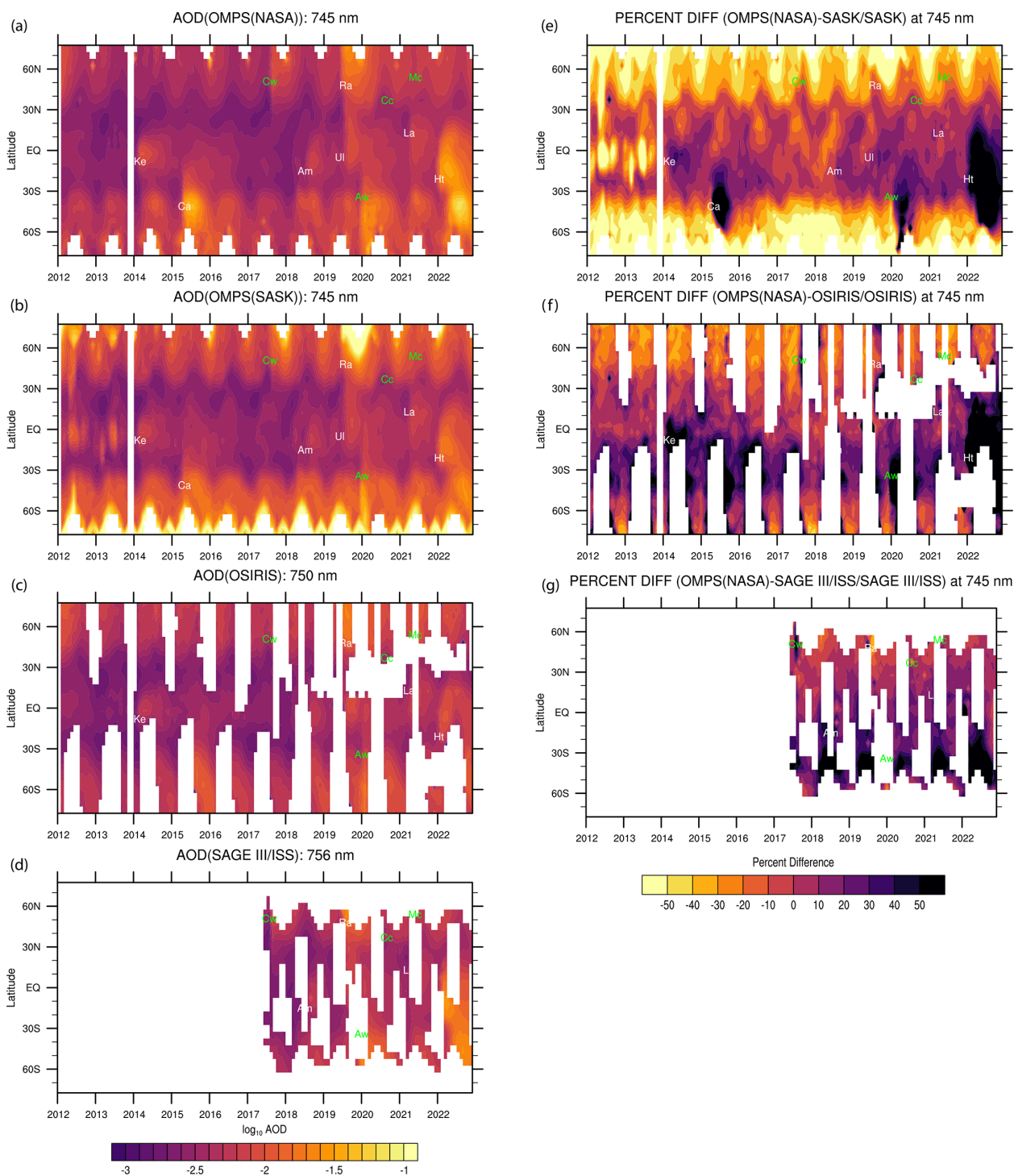


**Figure 3.** SAOD time series. (a) Time series of SAOD (latitude–time) for OMPS(NASA) at 745 nm. (b) Same as panel (a) but for OMPS(SASK). (c) Same as panel (a) but for OSIRIS at 750 nm. (d) Same as panel (a) but for SAGE III/ISS at 756 nm. Panel (d) shows the percent difference of SAOD time series between OMPS(NASA) (a) and OMPS(SASK) (b), panel (e) illustrates the percent difference of SAOD between OMPS(NASA) (a) and OSIRIS (c), and panel (f) shows the percent difference between OMPS(NASA) and SAGE III/ISS. Major volcanic eruptions (white) and wildfire events (green) with an abbreviated two-letter code and their respective latitude and time of occurrence are listed here. The event names shown are Kelud (Ke), Calbuco (Cb), Canadian wildfire (Cw), Ambae (Am), Raikoke (Rk), Ulawun (Ul), Australian wildfire (Aw), California Creek fire (Cc), La Soufriere (La), McKay Creek fire (Mc), and Hunga Tonga (Ht).

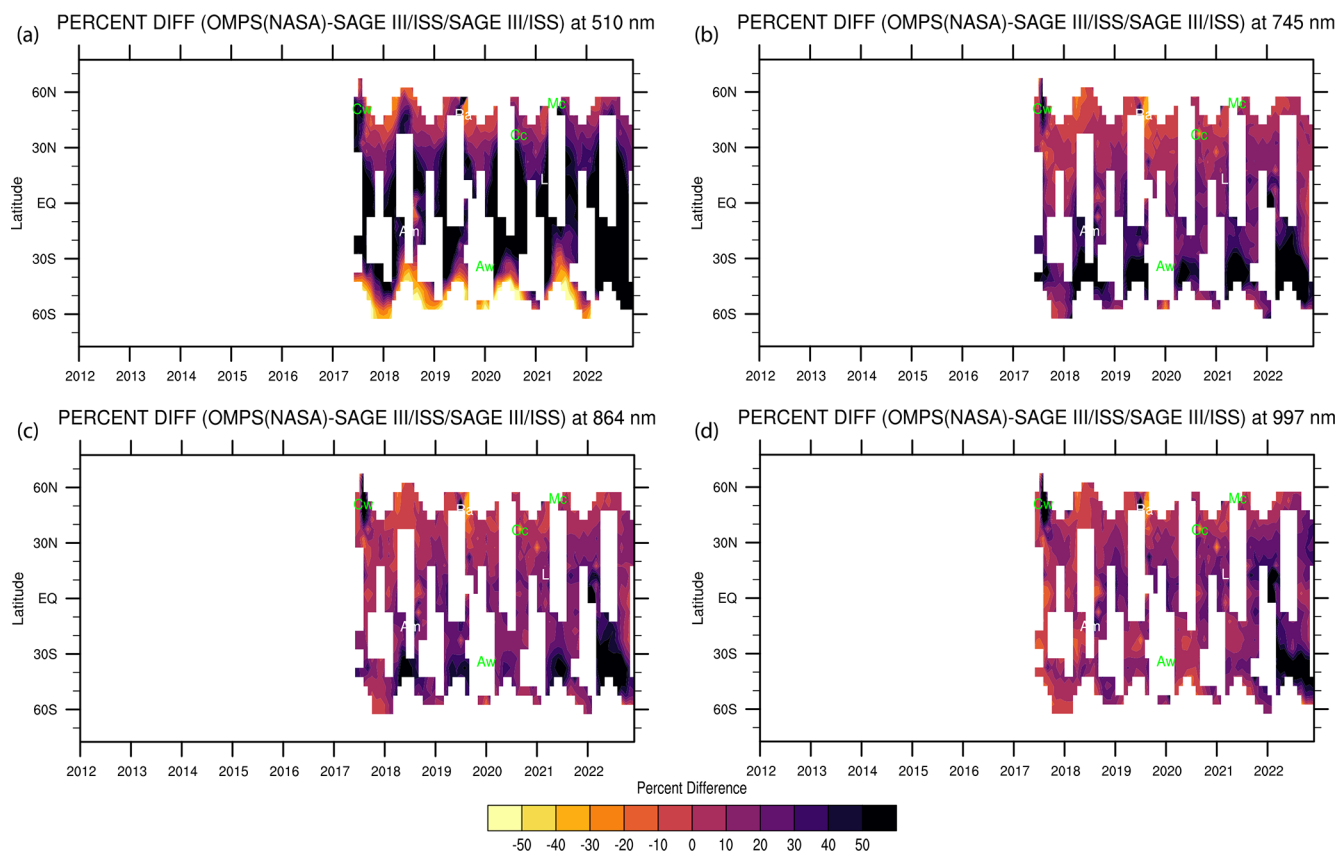


**Figure 4.** SAOD time series. Panel (a) shows the percent difference of SAOD time series between OMPS(NASA) and SAGE III at 510 nm, panel (b) the percent difference of SAOD time series between OMPS(NASA) and SAGE III at 745 nm, panel (c) the percent difference of SAOD time series between OMPS(NASA) and SAGE III at 864 nm, and panel (d) the percent difference of SAOD time series between OMPS(NASA) and SAGE III at 997 nm. Note that for the percent difference we use 510, 745, 864, and 997 nm from OMPS(NASA) and 521, 756, 869, and 1022 nm from SAGE III/ISS. Major volcanic eruptions (white) and wildfire events (green) are the same as those in Fig. 3.

wavelength measurements are unable to provide accurate information for inferring particle size.

### 3.3 Evaluating OMPS(NASA) multiwavelength measurements in the context of GloSSAC

For comparison purposes, we initially generated the zonally averaged aerosol extinction coefficient profiles of OMPS(NASA) and gridded them to the same spatial resolution as GloSSAC ( $5^\circ$  latitude resolution). Given that GloSSAC has a higher altitude resolution (0.5 km) than OMPS (1 km), we utilized it at the OMPS altitude resolution to avoid any interpolation along altitudes. While OSIRIS and CALIPSO have been components of GloSSAC version 2.22, the unavailability of CALIPSO data since January 2022 and the decreased coverage of OSIRIS resulted in GloSSAC relying predominantly on SAGE III/ISS since January 2022. We utilized the publicly available GloSSAC version 2.22 data (NASA/LARC/SD/ASDC, 2024) for the analyses. In our analysis, we first selected data for June 2017, representing a relatively stable period, and another case follow-

ing the Hunga Tonga eruption. Figure 6a, b depict the percent difference of OMPS(NASA) and GloSSAC at 525 and 1020 nm for June 2017 for a relatively background stratosphere. While reasonable agreement between OMPS(NASA) and GloSSAC was observed at 1020 nm ( $\pm 20\%$ ) except in the lower tropical stratosphere, significant discrepancies between the two data sets persisted at 525 nm. Similar differences were noted between the tropopause and approximately 24 km in the tropics and at the southern mid-latitudes.

For the data following the Hunga Tonga eruption in January 2022, we conducted a similar comparison for April 2022 (Fig. 6c, d), by which time the volcanic plume had largely dispersed. We note that the overestimation of OMPS(NASA) persisted in both the 525 and 1020 nm channels between the tropopause and approximately 25 km. Interestingly, at the peak of the aerosol layer, OMPS(NASA) underestimated GloSSAC by about 40%, while it overestimated GloSSAC below the peak of the aerosol layer by about 50% or more, exceeding the permissible limits ( $\pm 20\%$ ) between different data sets in the context of GloSSAC. The underestimation at the peak could be attributed to the fixed particle size distri-

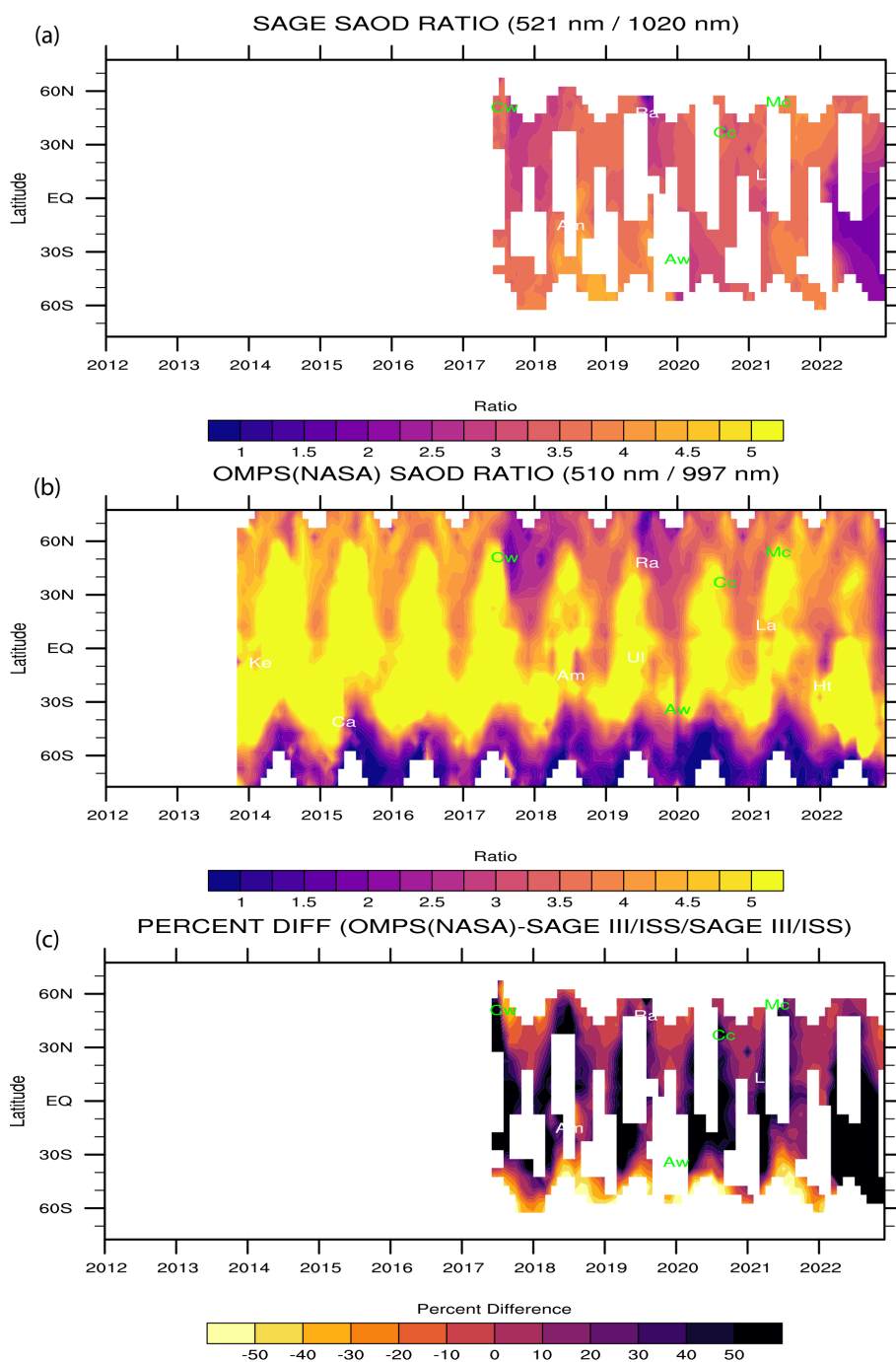


**Figure 5.** SAOD ratio time series. Panel (a) shows the SAOD ratio between 521 and 1020 nm from SAGE III/ISS, panel (b) shows the SAOD ratio between 510 and 997 nm from OMPS(NASA), and panel (c) shows the percent difference of SAOD ratios between (a) SAGE III/ISS and (b) OMPS(NASA). Major volcanic eruptions (white) and wildfire events (green) are the same as those in Fig. 3.

bution assumption, while the cause of the difference below the peak could be the difference in the retrieval algorithms between OMPS(NASA) and OMPS(SASK) and/or not converging the OMPS(NASA) product properly below the peak due to the retrieval technique and the number of iterations.

In addition to evaluating the aerosol extinction coefficient, we computed the SAOD as described in Sect. 3.1 (Fig. 3). Figure 7a–d show latitude–time plots of the OMPS(NASA) SAOD at 510 and 997 nm and GloSSAC version 2.22 at 525 and 1020 nm, highlighting aerosol enhancements after major events. However, Fig. 7e reveals consistent overestima-

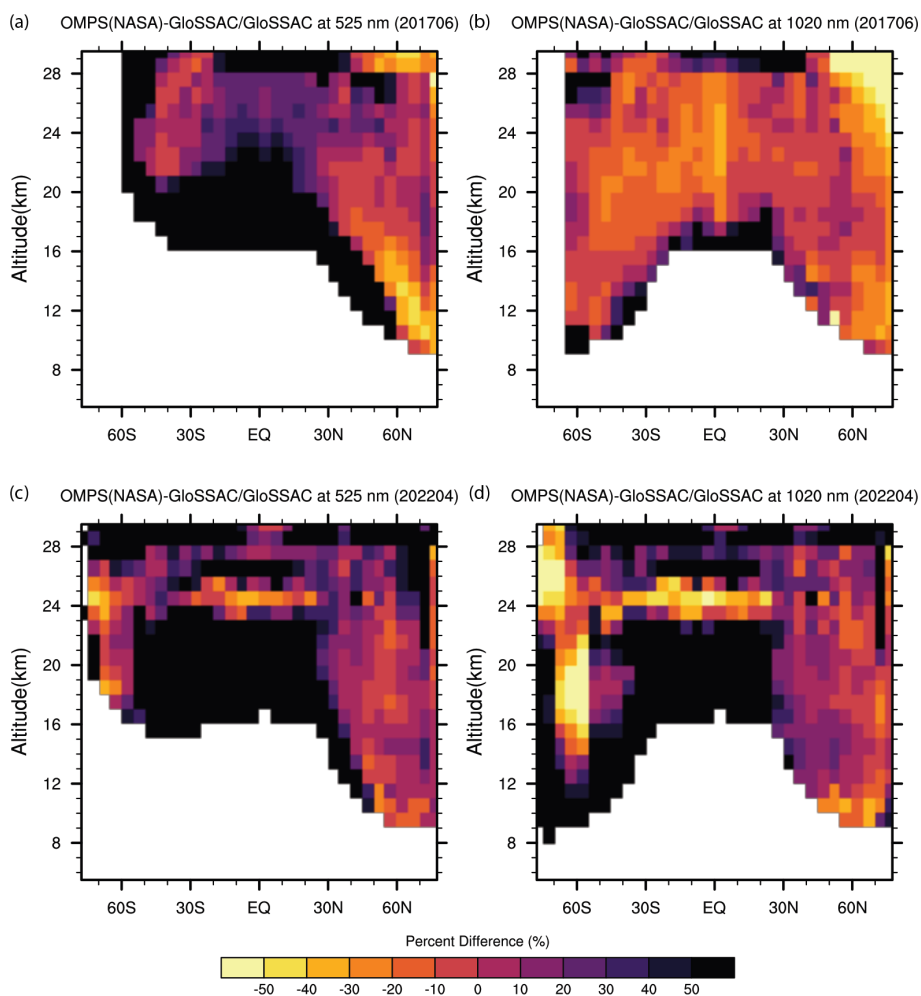


**Figure 6.** Zonal monthly averaged percent difference of OMPS(NASA) and GloSSAC (version 2.22) for 525 and 1020 nm in an altitude–latitude plot. Panels (a) and (b) are for June 2017 and panels (c) and (d) are for April 2022 following the Hunga Tonga eruption.

tion of SAOD by OMPS(NASA) at 510 nm, regardless of volcanic or fire activity, suggesting that it is unsuitable for GloSSAC. While the agreement between OMPS(NASA) and GloSSAC at 1020 nm (Fig. 7f) is better, significant overestimations follow major events, indicating potential issues with OMPS(NASA), particularly under perturbed conditions.

We also compared SAOD ratios (510/997 nm for OMPS and 525/1020 nm for GloSSAC; Fig. 7g, h) to infer particle size variations. Previous studies have demonstrated how the aerosol extinction coefficient ratios can be leveraged to infer particle sizes using the SAGE series of measurements (e.g., Thomason et al., 2021; Wrana et al., 2021; Knepp et al., 2024). We only considered the time series from 2017 through 2022 due to the availability of SAGE III/ISS multiwavelength measurements from 2017. The OMPS ratios provide limited size information, while the GloSSAC ratios offer valuable insights into particle size changes after volcanic and fire events. For instance, the Canadian wildfire and Hunga Tonga events suggest larger particles, while Am-

bae and Ulawun indicate smaller particles. This underscores the importance of multiwavelength measurements, like those from SAGE, in capturing aerosol size information critical for GloSSAC.

#### 4 Stratospheric aerosol effective radiative forcing and the associated surface temperature response

Figure 8 shows the  $\Delta$ SAOD averaged between 60° S and 60° N together with the corresponding global mean ERF estimates (see Sect. 2.4) for the period 2017–2022, when the  $\Delta$ SAOD from OMPS(NASA) is significantly different from other measurements, particularly following the Hunga Tonga eruption in January 2022. The largest discrepancy occurs in August 2022, when the OMPS(NASA) SAOD peak is 0.036, whereas the OMPS(SASK), SAGE III/ISS, GloSSAC, and OSIRIS SAOD values are approximately 0.013, 0.01, 0.01, and 0.006, respectively. On average, the  $\Delta$ SAOD difference between OMPS(NASA) and other measurements

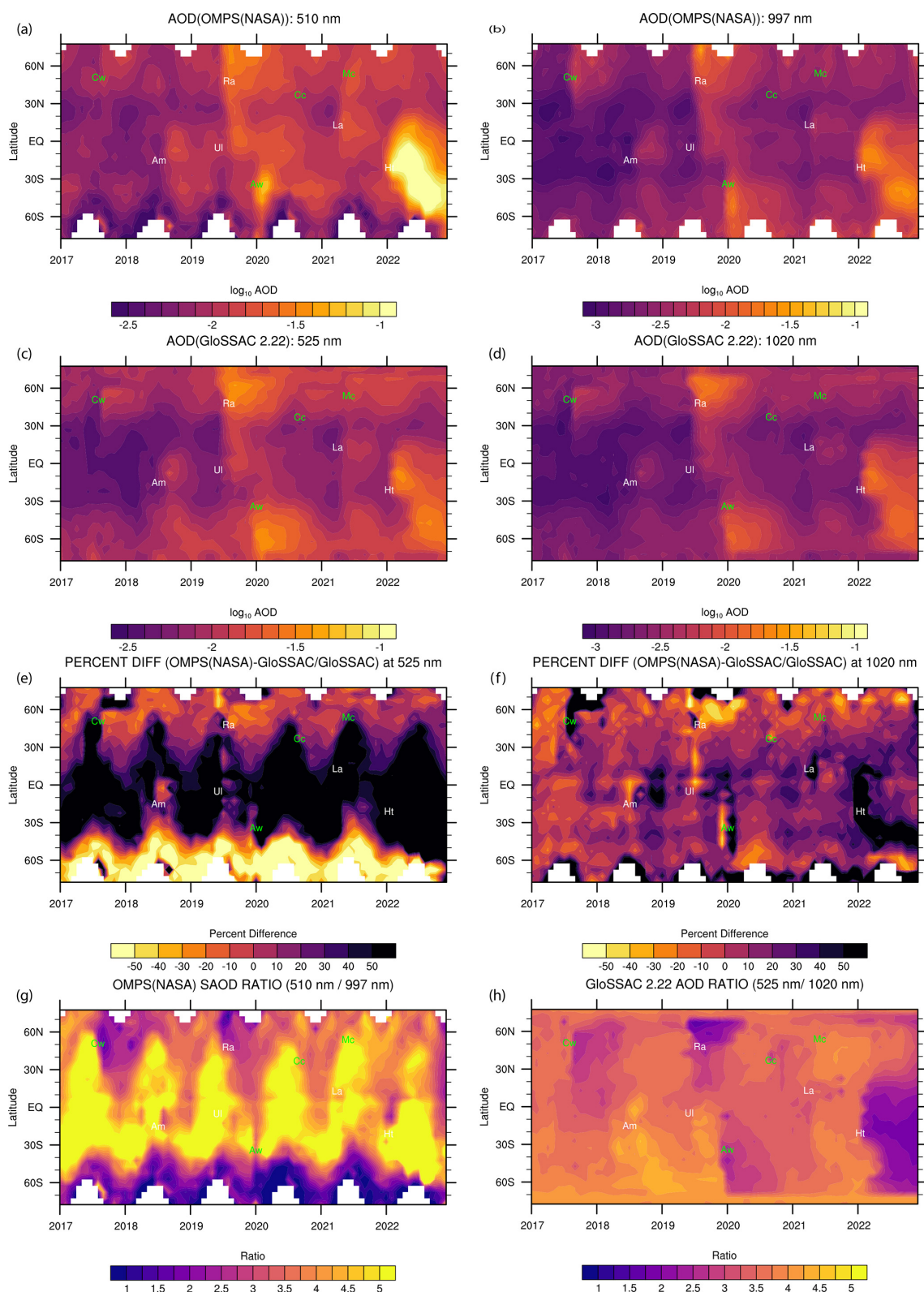


**Figure 7.** Latitude–time dependence of zonally averaged SAOD from OMPS(NASA) and GloSSAC (version 2.22). OMPS(NASA) SAODs are computed for 510 and 997 nm (a, b), while GloSSAC SAODs are computed for 525 and 1020 nm (c, d). Percent differences between OMPS(NASA) and GloSSAC are also shown in panel (e) for 525 nm and panel (f) for 1020 nm. The ratio between 510 and 997 nm of the OMPS(NASA) SAOD is shown in panel (g), while panel (h) shows the ratio between 525 and 1020 nm of GloSSAC version 2.22 for the same time period. Major volcanic eruptions (white) and wildfire events (green) are the same as those in Fig. 3.

is about a factor of 3. Additionally, the discrepancy in the OMPS(SASK)  $\Delta$ SAOD, relative to SAGE III/ISS and GloSSAC, is largely caused by an overestimation of the extinction coefficient poleward of  $40^\circ$  S and  $40^\circ$  N as shown in Fig. 3b. We then estimated the ERF from the  $\Delta$ SAOD time series using Eq. (1) (Marshall et al., 2020). In August 2022, at the peak of the OMPS(NASA)  $\Delta$ SAOD, the OMPS(NASA) ERF of  $-0.73 \text{ W m}^{-2}$  is stronger by a factor of about 3 compared to SAGE III/ISS/GloSSAC, as shown in Fig. 8b. This difference in ERF could be significant in terms of the surface temperature impact (e.g., Ridley et al., 2014). Ridley et al. (2014) used a simple climate model to compute the global volcanic aerosol forcing between 2000 and 2014, estimating it at  $-0.19 \pm 0.09 \text{ W m}^{-2}$ , which translates into an estimated global cooling of 0.05 to  $0.12^\circ\text{C}$ .

We utilized the FaIR model to estimate the global mean surface temperature response from the estimated monthly ERF time series shown in Fig. 8b (see Sect. 2.4). These results clearly indicate a cooling of about  $0.092 \text{ K}$  induced by the OMPS(NASA) ERF compared to coolings of  $0.061$ ,  $0.039$ ,  $0.042$ , and  $0.041 \text{ K}$  for OMPS(SASK), OSIRIS, SAGE III/ISS, and GloSSAC, respectively, for August 2022. The global surface temperature continues to cool even months after the peak of the OMPS(NASA) SAOD in August 2022, which is attributed to the higher heat capacity of the ocean that results in a slow temperature response. For December 2022, we note coolings of  $0.105$ ,  $0.067$ ,  $0.042$ ,  $0.046$ , and  $0.044 \text{ K}$  for OMPS(NASA), OMPS(SASK), OSIRIS, SAGE III/ISS, and GloSSAC, respectively. The temperature response from OMPS(NASA) exceeds a factor of 2 relative to SAGE III/ISS and GloSSAC.

For the Hunga Tonga eruption, we also calculated the difference between the peak cooling in December 2022 and the mean 2021 temperature response from Fig. 8c. The OMPS(NASA) ERF induced a cooling of  $0.064 \text{ K}$  compared to coolings of  $0.021$ ,  $0.008$ ,  $0.018$ , and  $0.017 \text{ K}$  for OMPS(SASK), OSIRIS, SAGE III/ISS, and GloSSAC, respectively (Fig. 8c). On average, over the 2017–2022 time period, we estimate that SAOD forcing cooled the climate by  $0.031$ ,  $0.034$ ,  $0.022$ ,  $0.019$ , and  $0.019 \text{ K}$  in OMPS(NASA), OMPS(SASK), OSIRIS, SAGE III/ISS, and GloSSAC, respectively. Thus, the OMPS(NASA) extinction coefficient product must be used with caution in stratospheric aerosol and climate studies, particularly following major volcanic events such as the Hunga Tonga eruption.

## 5 Summary and conclusions

We have examined and assessed two publicly available OMPS aerosol extinction coefficient products, i.e., OMPS(NASA) and OMPS(SASK), with other available space-based measurements in the context of the GloSSAC framework. The analysis thus far has revealed persistent disparities in the aerosol extinction coefficient, especially in

the OMPS(NASA) product, demonstrating overestimation ( $> 50\%$ ) following the Hunga Tonga eruption at  $745 \text{ nm}$ , which aligns with the findings of Bourassa et al. (2023). While Bourassa et al. (2023) focused on the period following the Hunga Tonga eruption and specifically at the  $745 \text{ nm}$  wavelength, our analysis extends back to the year 2012, when OMPS began its measurements. This extended time frame has enabled us to assess the consistent nature of these differences between OMPS(NASA) and other data sets, particularly in the context of volcanic eruptions and fire events. Furthermore, we leveraged this situation to evaluate OMPS(NASA) against OMPS(SASK), utilizing data from a few volcanic eruptions during that period, such as Kelud on 13 February 2014 at  $8^\circ$  S and Calbuco on 22 April 2015 at  $41^\circ$  S, and OMPS(NASA) significantly overestimates ( $> 50\%$ ) the aerosol extinction coefficient for these events as well.

In addition to the significant differences in the OMPS(NASA) aerosol extinction coefficient at  $745 \text{ nm}$ , other wavelengths from OMPS(NASA) show inconsistency across different channels. OMPS(NASA) provides the aerosol extinction coefficient data at multiple wavelengths, giving us the opportunity to compare the measurements at  $510$ ,  $745$ ,  $869$ , and  $997 \text{ nm}$  with those at  $521$ ,  $756$ ,  $864$ , and  $1020 \text{ nm}$  from SAGE III/ISS. The comparison between OMPS at  $510 \text{ nm}$  and SAGE III/ISS at  $521 \text{ nm}$  reveals significant differences, with OMPS(NASA) consistently exhibiting a high bias ( $> 50\%$ ) throughout the record, regardless of any perturbed events. However, the overall agreement improves towards longer wavelengths. Despite this, overestimation of the OMPS(NASA) aerosol extinction coefficient persists relative to SAGE III/ISS following major perturbed events, showing a high bias in OMPS(NASA) measurements during periods of elevated stratospheric aerosol loading. Additionally, we have computed the SAOD from OMPS(NASA) and assessed it with other products. The results clearly exhibit overestimation ( $> 50\%$ ) of the SAOD following major volcanic events. While the permissible differences between the instruments used in the GloSSAC framework are  $\pm 20\%$  (Thomason et al., 2018; Kovilakam et al., 2020), the differences exceeding  $50\%$  or more in most of the perturbed cases make the OMPS(NASA) product unsuitable for GloSSAC.

Additionally, we assessed the consistency in the OMPS(NASA) SAOD ratio between  $510$  and  $997 \text{ nm}$  compared to the SAGE III/ISS–GloSSAC SAOD ratio between  $525$  and  $1020 \text{ nm}$  for the period between 2017 and 2022, when SAGE III/ISS multiwavelength measurements are available. The OMPS SAOD ratios do not provide any meaningful information, suggesting that the  $510$  and  $997 \text{ nm}$  wavelengths cannot be used to infer any size information (Fig. 7g). In contrast, the SAGE III/ISS–GloSSAC–SAOD ratios exhibit consistency following each perturbed event, providing valuable insights into how ratios change following each volcanic or fire event, particularly after the Canadian

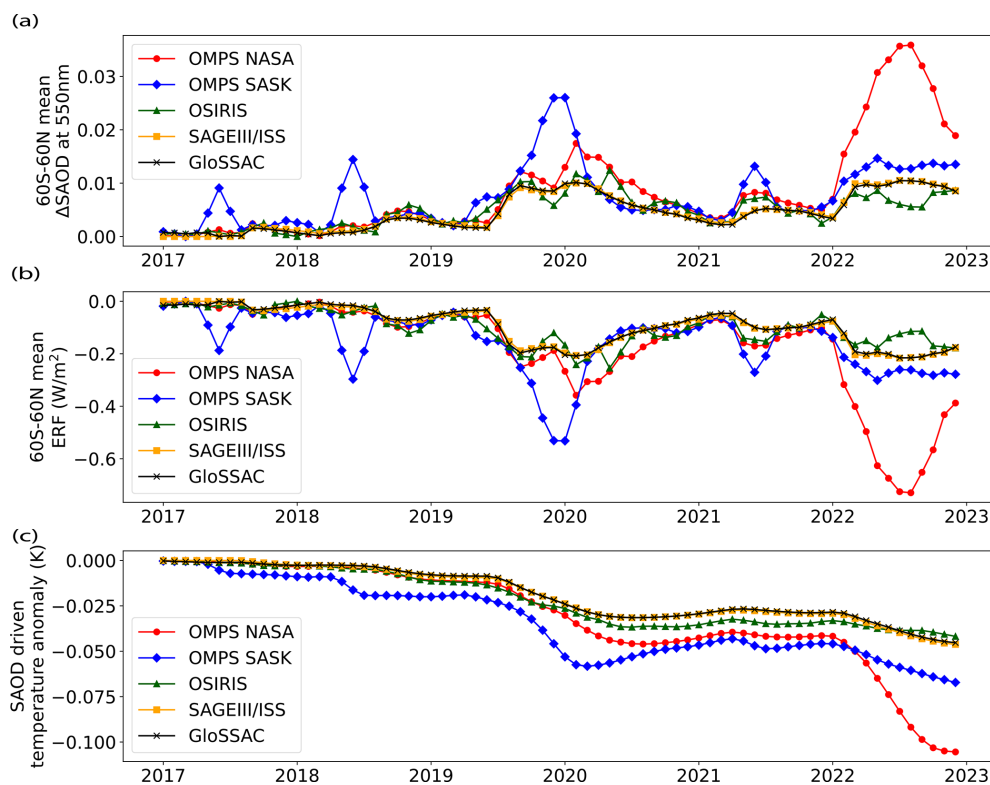


**Figure 8.** Time series of near-global 550 nm  $\Delta$ SAOD (a), effective radiative forcing (b), and temperature response (c) from OMPS(NASA), OMPS(SASK), OSIRIS, SAGE III/ISS, and GloSSAC. To compute  $\Delta$ SAOD at 550 nm from 745 nm OMPS(NASA), OMPS(SASK), and OSIRIS, we used a constant Ångström coefficient of 2.393, while for SAGE III/ISS and GloSSAC we used 1.97 to convert the extinction from 525 to 550 nm. The resulting monthly surface temperature response in panel (c) is estimated from the FaIR model.

wildfire, Ambae, Ulawun, Raikoke, the Australian wildfire, and Hunga Tonga (Fig. 7h).

Moreover, the aerosol extinction coefficients across different channels of OMPS(NASA) (510, 745, 869, and 997 nm) are not consistent, particularly following perturbed events. Therefore, it is important to emphasize that, while limb-scatter measurements are valuable, their ability to produce reliable multiwavelength aerosol extinction measurements remains limited. Following volcanic and smoke events in the stratosphere, the quality of these measurements can be affected, which can affect the accuracy of aerosol extinction coefficient ratios and the inference of aerosol size information. In contrast, the multiwavelength aerosol extinction coefficient from solar occultation measurements, such as SAGE, plays a vital role in providing important multiwavelength information on aerosol particle size-related details in GloSSAC.

We also estimated the SAOD-driven ERF from each instrument, finding that the OMPS(NASA)-driven ERF has a larger impact on radiative forcing compared to the other data sets. At the SAOD peak in August 2022, the OMPS(NASA)-induced ERF is  $-0.73 \text{ W m}^{-2}$ , which is about 3 times higher than the ERF from SAGE III/ISS and GloSSAC (Fig. 8b). We used the ERF time series to estimate the surface tem-

perature response using the FaIR model. The results show a significant cooling of approximately 0.092 K induced by the OMPS(NASA) ERF compared to coolings of 0.061, 0.039, 0.042, and 0.041 K for OMPS(SASK), OSIRIS, SAGE II/ISS, and GloSSAC, respectively, for August 2022 (Fig. 8c).

Based on our analysis, the OMPS(NASA) product consistently exhibits a high bias (exceeding 50%), particularly in the aftermath of perturbed events, and in the context of GloSSAC the bias exceeds the allowable differences between the instruments ( $\pm 20\%$ ). In contrast, OMPS(SASK) demonstrates improved agreement with other space-based measurements. While OMPS(SASK) aligns reasonably well (within  $\pm 20\%$ ) with SAGE III/ISS at 745 nm, it overestimates extinction coefficients poleward of  $40^\circ \text{ S}$  and  $40^\circ \text{ N}$ , which is potentially due to cloud contamination in the OMPS(SASK) data and a seasonal cycle. Enhancing the cloud-clearing algorithm and potentially removing the seasonal cycle may address this issue and improve the data quality in these regions. Additionally, we note an overestimation of OMPS(SASK) extinction in the tropics in the first couple of years of OMPS operations. Excluding the data quality issues in the first couple of years, the OMPS(SASK) product appears usable in GloSSAC. However, challenges arise when converting the OMPS(SASK) aerosol extinction coefficient from 745 to 525

and 1020 nm, as GloSSAC provides the aerosol extinction coefficient data at these wavelengths. Previous studies employed a constant Ångström exponent for this conversion (Rieger et al., 2015), but this approach may not be suitable, especially considering the curvature in the aerosol spectrum following perturbed events such as volcanic eruptions or wildfires. To address this, we plan to explore the potential of using a pseudo-Ångström exponent, following the methodology developed in Kovilakam et al. (2020, 2023). This process entails utilizing the OMPS(SASK) aerosol extinction coefficient at 745 nm in conjunction with the SAGE III/ISS aerosol extinction coefficient at 525 and 1020 nm to establish a monthly median pseudo-Ångström exponent climatology. Although employing a monthly median climatology proves effective, it may not sufficiently capture variations in the aerosol extinction coefficient at each wavelength, especially following a volcanic eruption or wildfire event, as highlighted in Kovilakam et al. (2020). To address this limitation, we intend to refine the method by introducing a time-varying pseudo-Ångström exponent when both OMPS(SASK) and SAGE III/ISS data are available. For data prior to June 2017, where we did not have any SAGE measurements, we propose reverting to using a monthly median climatology of the pseudo-Ångström exponent.

In addition to the differences between OMPS(SASK) and SAGE III/ISS mentioned above, some differences between OMPS(SASK) and SAGE III/ISS persist, especially at the peak of the aerosol layer following the Hunga Tonga eruption. Our future work will include addressing this issue by investigating the sensitivity of the OMPS(SASK) algorithm to the particle size distribution assumption, which is currently implemented as a constant lognormal size distribution. We plan to test the algorithm with variable size distributions from SAGE III/ISS (e.g., Knepp et al., 2024; Ernest et al., 2024) to determine whether this assumption contributes to the underestimation of the aerosol extinction coefficient at the peak of any enhanced aerosol layer. Preliminary studies suggest that seeding the retrieval of limb-scatter measurements with size distributions inferred from solar occultation measurements improves the quality of the limb-scatter instrument's derived aerosol products. It may be possible to extend this capacity to a post-occultation future, but substantial and obvious hurdles will need to be overcome before this can be expected to result in an acceptable data set for climate research and data sets like GloSSAC.

As highlighted previously, the SAGE series of measurements plays a pivotal role in GloSSAC, offering indispensable data from 1979 to the present, albeit with a hiatus between August 2005 and May 2017. With the aim of developing stratospheric aerosol properties for the upcoming 7th phase of the Coupled Model Intercomparison Project (CMIP7) forcing, GloSSAC has been designated as the observational data set, spanning the satellite era from 1979 onward. Therefore, the continued maintenance of the GloSSAC data record is essential, serving the crucial purpose of quan-

tifying uncertainties in climate forcing within CMIP7 and independently assessing the output of climate models.

**Data availability.** The GloSSAC v2.22 netCDF file is available from the NASA Atmospheric Data Center (<https://doi.org/10.5067/GLOSSAC-L3-V2.22>; NASA/LARC/SD/ASDC, 2024). The SAGE III/ISS and CALIOP data used in this study are available from the NASA Atmospheric Data Center, while the OSIRIS version 7.2 data can be downloaded from <https://research-groups.usask.ca/osiris/data-products.php#OSIRISLevel2DataProducts> (University of Saskatchewan, 2025).

**Author contributions.** MK and LWT developed the idea and methodology used in this paper. MK carried out all the analyses except for the ERF and surface temperature analyses, which were performed by MV and TA, while TNK participated in the scientific discussion. MK wrote the manuscript, while all the authors reviewed the manuscript and provided advice on it and its figures.

**Competing interests.** The contact author has declared that none of the authors has any competing interests.

**Disclaimer.** Publisher's note: Copernicus Publications remains neutral with regard to jurisdictional claims made in the text, published maps, institutional affiliations, or any other geographical representation in this paper. While Copernicus Publications makes every effort to include appropriate place names, the final responsibility lies with the authors.

**Acknowledgements.** We acknowledge the support of the NASA Science Mission Directorate and the SAGE II and III/ISS mission teams. The SAGE mission is supported by the NASA Science Mission Directorate. ADNET personnel are supported by a RSES contract and NASA grant no. 80NSSC 24K1185. Magali Verkerk acknowledges support from the Faculty of Environment, Science and Economy of the University of Exeter through a doctoral scholarship. Thomas Aubry acknowledges support from the Coupled Model Intercomparison Project International Project Office. We also acknowledge the International Space Science Institute (ISSI) team of project 23-579, "Perspectives on Stratospheric Aerosol Observations", for their valuable scientific discussions.

**Financial support.** This research has been supported by the Aeronautics Research Mission Directorate (grant no. 80NSSC 24K1185). Magali Verkerk was supported by the Faculty of Environment, Science and Economy of the University of Exeter through a doctoral scholarship. Thomas Aubry was supported by the Coupled Model Intercomparison Project International Project Office.

**Review statement.** This paper was edited by Suvarna Fadnavis and reviewed by two anonymous referees.

## References

- Aquila, V., Oman, L. D., Stolarski, R., Douglass, A. R., and Newman, P. A.: The Response of Ozone and Nitrogen Dioxide to the Eruption of Mt. Pinatubo at Southern and Northern Midlatitudes, *J. Atmos. Sci.*, 70, 894–900, <https://doi.org/10.1175/JAS-D-12-0143.1>, 2013.
- Aubry, T. J., Toohey, M., Marshall, L., Schmidt, A., and Jellinek, A. M.: A New Volcanic Stratospheric Sulfate Aerosol Forcing Emulator (EVA\_H): Comparison With Interactive Stratospheric Aerosol Models, *J. Geophys. Res.-Atmos.*, 125, e2019JD031303, <https://doi.org/10.1029/2019JD031303>, 2020.
- Berdahl, M. and Robock, A.: Northern Hemispheric cryosphere response to volcanic eruptions in the Paleoclimate Modeling Intercomparison Project 3 last millennium simulations, *J. Geophys. Res.-Atmos.*, 118, 12359–12370, <https://doi.org/10.1002/2013JD019914>, 2013.
- Bourassa, A. E., Rieger, L. A., Lloyd, N. D., and Degenstein, D. A.: Odin-OSIRIS stratospheric aerosol data product and SAGE III intercomparison, *Atmos. Chem. Phys.*, 12, 605–614, <https://doi.org/10.5194/acp-12-605-2012>, 2012.
- Bourassa, A. E., Rieger, L. A., Zawada, D. J., Khaykin, S., Thomason, L. W., and Degenstein, D. A.: Satellite Limb Observations of Unprecedented Forest Fire Aerosol in the Stratosphere, *J. Geophys. Res.-Atmos.*, 124, 9510–9519, <https://doi.org/10.1029/2019JD030607>, 2019.
- Bourassa, A. E., Zawada, D. J., Rieger, L. A., Warnock, T. W., Toohey, M., and Degenstein, D. A.: Tomographic Retrievals of Hunga Tonga-Hunga Ha’apai Volcanic Aerosol, *Geophys. Res. Lett.*, 50, e2022GL101978, <https://doi.org/10.1029/2022GL101978>, 2023.
- Chen, Z., Bhartia, P. K., Loughman, R., Colarco, P., and DeLand, M.: Improvement of stratospheric aerosol extinction retrieval from OMPS/LP using a new aerosol model, *Atmos. Meas. Tech.*, 11, 6495–6509, <https://doi.org/10.5194/amt-11-6495-2018>, 2018.
- Deshler, T., Hervig, M. E., Hofmann, D. J., Rosen, J. M., and Liley, J. B.: Thirty years of in situ stratospheric aerosol size distribution measurements from Laramie, Wyoming (41°N), using balloon-borne instruments, *J. Geophys. Res.-Atmos.*, 108, 4167, <https://doi.org/10.1029/2002JD002514>, 2003.
- Deshler, T., Luo, B., Kovilakam, M., Peter, T., and Kalnajs, L. E.: Retrieval of Aerosol Size Distributions From In Situ Particle Counter Measurements: Instrument Counting Efficiency and Comparisons With Satellite Measurements, *J. Geophys. Res.-Atmos.*, 124, 5058–5087, <https://doi.org/10.1029/2018JD029558>, 2019.
- Ernest, N., Thomason, L. W., and Deshler, T.: Producing aerosol size distributions consistent with optical particle counters measurements using space-based measurements of aerosol extinction coefficient, *Atmos. Meas. Tech. Discuss.* [preprint], <https://doi.org/10.5194/amt-2024-62>, in review, 2024.
- Eyring, V., Bony, S., Meehl, G. A., Senior, C. A., Stevens, B., Stouffer, R. J., and Taylor, K. E.: Overview of the Coupled Model Intercomparison Project Phase 6 (CMIP6) experimental design and organization, *Geosci. Model Dev.*, 9, 1937–1958, <https://doi.org/10.5194/gmd-9-1937-2016>, 2016.
- Flynn, L. E., Seftor, C. J., Larsen, J. C., and Xu, P.: The ozone mapping and profiler suite, in: *Earth science satellite remote sensing*, Springer, 279–296, online ISBN 978-3-540-37293-6, [https://doi.org/10.1007/978-3-540-37293-6\\_15](https://doi.org/10.1007/978-3-540-37293-6_15), 2006.
- Forster, P., Storelvmo, T., Armour, K., Collins, W., Dufresne, J.-L., Frame, D., Lunt, D., Mauritsen, T., Palmer, M., Watanabe, M., Wild, M., and Zhang, H.: The Earth’s Energy Budget, Climate Feedbacks, and Climate Sensitivity. In *Climate Change 2021: The Physical Science Basis. Contribution of Working Group I to the Sixth Assessment Report of the Intergovernmental Panel on Climate Change*, edited by: Masson-Delmotte, V., Zhai, P., Pirani, A., Connors, S. L., Péan, C., Berger, S., Caud, N., Chen, Y., Goldfarb, L., Gomis, M. I., Huang, M., Leitzell, K., Lonnoy, E., Matthews, J. B. R., Maycock, T. K., Waterfield, T., Yelekçi, O., Yu, R., and Zhou, B., Cambridge University Press, Cambridge, United Kingdom and New York, NY, USA, 923–1054, <https://doi.org/10.1017/9781009157896.009>, 2021.
- Fyfe, J. C., von Salzen, K., Cole, J. N. S., Gillett, N. P., and Vernier, J.-P.: Surface response to stratospheric aerosol changes in a coupled atmosphere–ocean model, *Geophys. Res. Lett.*, 40, 584–588, <https://doi.org/10.1002/grl.50156>, 2013.
- Hervig, M. and Deshler, T.: Evaluation of aerosol measurements from SAGE II, HALOE, and balloonborne optical particle counters, *J. Geophys. Res.-Atmos.*, 107, AAC 3-1–AAC 3-12, <https://doi.org/10.1029/2001JD000703>, 2002.
- Kar, J., Lee, K.-P., Vaughan, M. A., Tackett, J. L., Trepte, C. R., Winker, D. M., Lucker, P. L., and Getzewich, B. J.: CALIPSO level 3 stratospheric aerosol profile product: version 1.00 algorithm description and initial assessment, *Atmos. Meas. Tech.*, 12, 6173–6191, <https://doi.org/10.5194/amt-12-6173-2019>, 2019.
- Knepp, T. N., Kovilakam, M., Thomason, L., and Miller, S. J.: Characterization of stratospheric particle size distribution uncertainties using SAGE II and SAGE III/ISS extinction spectra, *Atmos. Meas. Tech.*, 17, 2025–2054, <https://doi.org/10.5194/amt-17-2025-2024>, 2024.
- Kovilakam, M., Thomason, L. W., Ernest, N., Rieger, L., Bourassa, A., and Millán, L.: The Global Space-based Stratospheric Aerosol Climatology (version 2.0): 1979–2018, *Earth Syst. Sci. Data*, 12, 2607–2634, <https://doi.org/10.5194/essd-12-2607-2020>, 2020.
- Kovilakam, M., Thomason, L., and Knepp, T.: SAGE III/ISS aerosol/cloud categorization and its impact on GloSSAC, *Atmos. Meas. Tech.*, 16, 2709–2731, <https://doi.org/10.5194/amt-16-2709-2023>, 2023.
- Krishnamohan, K.-P. S.-P., Bala, G., Cao, L., Duan, L., and Caldeira, K.: Climate system response to stratospheric sulfate aerosols: sensitivity to altitude of aerosol layer, *Earth Syst. Dynam.*, 10, 885–900, <https://doi.org/10.5194/esd-10-885-2019>, 2019.
- Lacis, A., Hansen, J., and Sato, M.: Climate forcing by stratospheric aerosols, *Geophys. Res. Lett.*, 19, 1607–1610, <https://doi.org/10.1029/92GL01620>, 1992.
- Leach, N. J., Jenkins, S., Nicholls, Z., Smith, C. J., Lynch, J., Cain, M., Walsh, T., Wu, B., Tsutsui, J., and Allen, M. R.: FaIRv2.0.0: a generalized impulse response model for climate uncertainty and future scenario exploration, *Geosci. Model Dev.*, 14, 3007–3036, <https://doi.org/10.5194/gmd-14-3007-2021>, 2021.
- Marshall, L. R., Smith, C. J., Forster, P. M., Aubry, T. J., Andrews, T., and Schmidt, A.: Large Variations in Volcanic Aerosol Forcing Efficiency Due to Eruption Source Parameters and

- Rapid Adjustments, *Geophys. Res. Lett.*, 47, e2020GL090241, <https://doi.org/10.1029/2020GL090241>, 2020.
- Mauldin, L. E., Zaun, N. H., McCormick, M. P., Guy, J. H., and Vaughn, W. R.: Stratospheric aerosol and gas experiment II instrument: A functional description, *Opt. Eng.*, 24, 307–312, <https://doi.org/10.1117/12.7973473>, 1985.
- McCormick, M., Hamill, P., Chu, W., Swisler, T., McMaster, L., and Pepin, T.: Satellite studies of the stratospheric aerosol, *B. Am. Meteorol. Soc.*, 60, 1038–1046, 1979.
- McLinden, C., Bourassa, A., Brohede, S., Cooper, M., Degenstein, D., Evans, W., Gattinger, R., Haley, C., Llewellyn, E., Lloyd, N., Loewen, P., Martin, R. V., McConnell, J. C., McDade I. C., Murtagh, D., Rieger, L., von Savigny, C., Sheese, P. E., Sioris, C. E., Solheim, B., and Strong, K.: OSIRIS: A decade of scattered light, *B. Am. Meteorol. Soc.*, 93, 1845–1863, 2012.
- Millar, R. J., Nicholls, Z. R., Friedlingstein, P., and Allen, M. R.: A modified impulse-response representation of the global near-surface air temperature and atmospheric concentration response to carbon dioxide emissions, *Atmos. Chem. Phys.*, 17, 7213–7228, <https://doi.org/10.5194/acp-17-7213-2017>, 2017.
- Mills, M. J., Schmidt, A., Easter, R., Solomon, S., Kinnison, D. E., Ghan, S. J., Neely III, R. R., Marsh, D. R., Conley, A., Bardeen, C. G., and Gettelman, A.: Global volcanic aerosol properties derived from emissions, 1990–2014, using CESM1(WACCM), *J. Geophys. Res.-Atmos.*, 121, 2332–2348, 2016.
- Myhre, G., Shindell, D., Bréon, F.-M., Collins, W., Fuglestedt, J., Huang, J., Koch, D., Lamarque, J.-F., Lee, D., Mendoza, B., Nakajima, T., Robock, A., Stephens, G., Takemura, T., and Zhang, H.: Anthropogenic and Natural Radiative Forcing. In: *Climate Change 2013: The Physical Science Basis. Contribution of Working Group I to the Fifth Assessment Report of the Intergovernmental Panel on Climate Change*, edited by: Stocker, T. F., Qin, D., Plattner, G.-K., Tignor, M., Allen, S. K., Doschung, J., Nauels, A., Xia, Y., Bex, V., and Midgley, P. M., Cambridge University Press, Cambridge, UK, 659–740, <https://doi.org/10.1017/CBO9781107415324.018>, 2013.
- NASA/LARC/SD/ASDC: Global Space-based Stratospheric Aerosol Climatology Version 2.22, NASA Langley Atmospheric Science Data Center DAAC [data set], <https://doi.org/10.5067/GLOSSAC-L3-V2.22>, 2024.
- Nicholls, Z., Meinshausen, M., Lewis, J., Corradi, M. R., Dorheim, K., Gasser, T., Gieseke, R., Hope, A. P., Leach, N. J., McBride, L. A., Quilcaille, Y., Rogelj, J., Salawitch, R. J., Samset, B. H., Sandstad, M., Shiklomanov, A., Skeie, R. B., Smith, C. J., Smith, S. J., Su, X., Tsutsui, J., Vega-Westhoff, B., and Woodard, D. L.: Reduced Complexity Model Intercomparison Project Phase 2: Synthesizing Earth System Knowledge for Probabilistic Climate Projections, *Earth's Future*, 9, e2020EF001900, <https://doi.org/10.1029/2020EF001900>, e2020EF001900 2020EF001900, 2021.
- Quaglia, I., Timmreck, C., Niemeier, U., Visioni, D., Pitari, G., Brodowsky, C., Brühl, C., Dhomse, S. S., Franke, H., Laakso, A., Mann, G. W., Rozanov, E., and Sukhodolov, T.: Interactive stratospheric aerosol models' response to different amounts and altitudes of SO<sub>2</sub> injection during the 1991 Pinatubo eruption, *Atmos. Chem. Phys.*, 23, 921–948, <https://doi.org/10.5194/acp-23-921-2023>, 2023.
- Ridley, D., Solomon, S., Barnes, J. E., Burlakov, V. D., Deshler, T., Dolgii, S. I., Herber, A. B., Nagai, T., Neely III, R. R., Nevzorov, A. V., Ritter, C., Sakai, T., Santer, B. D., Sato, M., Schmidt, A., Uchino, O., and Vernier, J. P.: Total volcanic stratospheric aerosol optical depths and implications for global climate change, *Geophys. Res. Lett.*, 41, 7763–7769, 2014.
- Rieger, L. A., Bourassa, A. E., and Degenstein, D. A.: Merging the OSIRIS and SAGE II stratospheric aerosol records, *J. Geophys. Res. Atmos.*, 120, 8890–8904, <https://doi.org/10.1002/2015JD023133>, 2015.
- Rieger, L. A., Zawada, D. J., Bourassa, A. E., and Degenstein, D. A.: A Multiwavelength Retrieval Approach for Improved OSIRIS Aerosol Extinction Retrievals, *J. Geophys. Res.-Atmos.*, 124, 7286–7307, <https://doi.org/10.1029/2018JD029897>, 2019.
- Rozanov, A., Pohl, C., Arosio, C., Bourassa, A., Bramstedt, K., Malinina, E., Rieger, L., and Burrows, J. P.: Retrieval of stratospheric aerosol extinction coefficients from sun-normalized Ozone Mapper and Profiler Suite Limb Profiler (OMPS-LP) measurements, *Atmos. Meas. Tech.*, 17, 6677–6695, <https://doi.org/10.5194/amt-17-6677-2024>, 2024.
- Smith, C. J., Forster, P. M., Allen, M., Leach, N., Millar, R. J., Passerello, G. A., and Regayre, L. A.: FAIR v1.3: a simple emissions-based impulse response and carbon cycle model, *Geosci. Model Dev.*, 11, 2273–2297, <https://doi.org/10.5194/gmd-11-2273-2018>, 2018.
- Stenchikov, G., Hamilton, K., Stouffer, R. J., Robock, A., Ramaswamy, V., Santer, B., and Graf, H.-F.: Arctic Oscillation response to volcanic eruptions in the IPCC AR4 climate models, *J. Geophys. Res.-Atmos.*, 111, D07107, <https://doi.org/10.1029/2005JD006286>, 2006.
- Taha, G., Loughman, R., Zhu, T., Thomason, L., Kar, J., Rieger, L., and Bourassa, A.: OMPS LP Version 2.0 multi-wavelength aerosol extinction coefficient retrieval algorithm, *Atmos. Meas. Tech.*, 14, 1015–1036, <https://doi.org/10.5194/amt-14-1015-2021>, 2021.
- Taha, G., Loughman, R., Colarco, P. R., Zhu, T., Thomason, L. W., and Jaross, G.: Tracking the 2022 Hunga Tonga-Hunga Ha'apai Aerosol Cloud in the Upper and Middle Stratosphere Using Space-Based Observations, *Geophys. Res. Lett.*, 49, e2022GL100091, <https://doi.org/10.1029/2022GL100091>, 2022.
- Thomason, L. W. and Vernier, J.-P.: Improved SAGE II cloud/aerosol categorization and observations of the Asian tropopause aerosol layer: 1989–2005, *Atmos. Chem. Phys.*, 13, 4605–4616, <https://doi.org/10.5194/acp-13-4605-2013>, 2013.
- Thomason, L. W., Moore, J. R., Pitts, M. C., Zawodny, J. M., and Chiou, E. W.: An evaluation of the SAGE III version 4 aerosol extinction coefficient and water vapor data products, *Atmos. Chem. Phys.*, 10, 2159–2173, <https://doi.org/10.5194/acp-10-2159-2010>, 2010.
- Thomason, L. W., Ernest, N., Millán, L., Rieger, L., Bourassa, A., Vernier, J.-P., Manney, G., Luo, B., Arfeuille, F., and Peter, T.: A global space-based stratospheric aerosol climatology: 1979–2016, *Earth Syst. Sci. Data*, 10, 469–492, <https://doi.org/10.5194/essd-10-469-2018>, 2018.
- Thomason, L. W., Kovilakam, M., Schmidt, A., von Savigny, C., Knepp, T., and Rieger, L.: Evidence for the predictability of changes in the stratospheric aerosol size following volcanic eruptions of diverse magnitudes using space-based instruments, *Atmos. Chem. Phys.*, 21, 1143–1158, <https://doi.org/10.5194/acp-21-1143-2021>, 2021.

- Timmreck, C., Mann, G. W., Aquila, V., Hommel, R., Lee, L. A., Schmidt, A., Brühl, C., Carn, S., Chin, M., Dhomse, S. S., Diehl, T., English, J. M., Mills, M. J., Neely, R., Sheng, J., Toohey, M., and Weisenstein, D.: The Interactive Stratospheric Aerosol Model Intercomparison Project (ISA-MIP): motivation and experimental design, *Geosci. Model Dev.*, 11, 2581–2608, <https://doi.org/10.5194/gmd-11-2581-2018>, 2018.
- University of Saskatchewan: Data Products, University of Saskatchewan [data set], <https://research-groups.usask.ca/osiris/data-products.php#OSIRISLevel2DataProducts>, last access: 3 January 2025.
- Wang, H. J. R., Damadeo, R., Flittner, D., Kramarova, N., Taha, G., Davis, S., Thompson, A. M., Strahan, S., Wang, Y., Froidevaux, L., Degenstein, D., Bourassa, A., Steinbrecht, W., Walker, K. A., Querel, R., Leblanc, T., Godin-Beekmann, S., Hurst, D., and Hall, E.: Validation of SAGE III/ISS Solar Occultation Ozone Products With Correlative Satellite and Ground-Based Measurements, *J. Geophys. Res.-Atmos.*, 125, e2020JD032430, <https://doi.org/10.1029/2020JD032430>, 2020.
- Wrana, F., von Savigny, C., Zalach, J., and Thomason, L. W.: Retrieval of stratospheric aerosol size distribution parameters using satellite solar occultation measurements at three wavelengths, *Atmos. Meas. Tech.*, 14, 2345–2357, <https://doi.org/10.5194/amt-14-2345-2021>, 2021.
- Zanchettin, D., Khodri, M., Timmreck, C., Toohey, M., Schmidt, A., Gerber, E. P., Hegerl, G., Robock, A., Pausata, F. S. R., Ball, W. T., Bauer, S. E., Bekki, S., Dhomse, S. S., LeGrande, A. N., Mann, G. W., Marshall, L., Mills, M., Marchand, M., Niemeier, U., Poulain, V., Rozanov, E., Rubino, A., Stenke, A., Tsigaridis, K., and Tummon, F.: The Model Intercomparison Project on the climatic response to Volcanic forcing (VolMIP): experimental design and forcing input data for CMIP6, *Geosci. Model Dev.*, 9, 2701–2719, <https://doi.org/10.5194/gmd-9-2701-2016>, 2016.
- Zawada, D. J., Rieger, L. A., Bourassa, A. E., and Degenstein, D. A.: Tomographic retrievals of ozone with the OMPS Limb Profiler: algorithm description and preliminary results, *Atmos. Meas. Tech.*, 11, 2375–2393, <https://doi.org/10.5194/amt-11-2375-2018>, 2018.